UNIVERSITY OF COPENHAGEN
FACULTY OF SCIENCE, DEPARTMENT OF FOOD

Robust NIR calibration at Novo Nordisk – Designing a downscaled dry granulation process

MSc project thesis

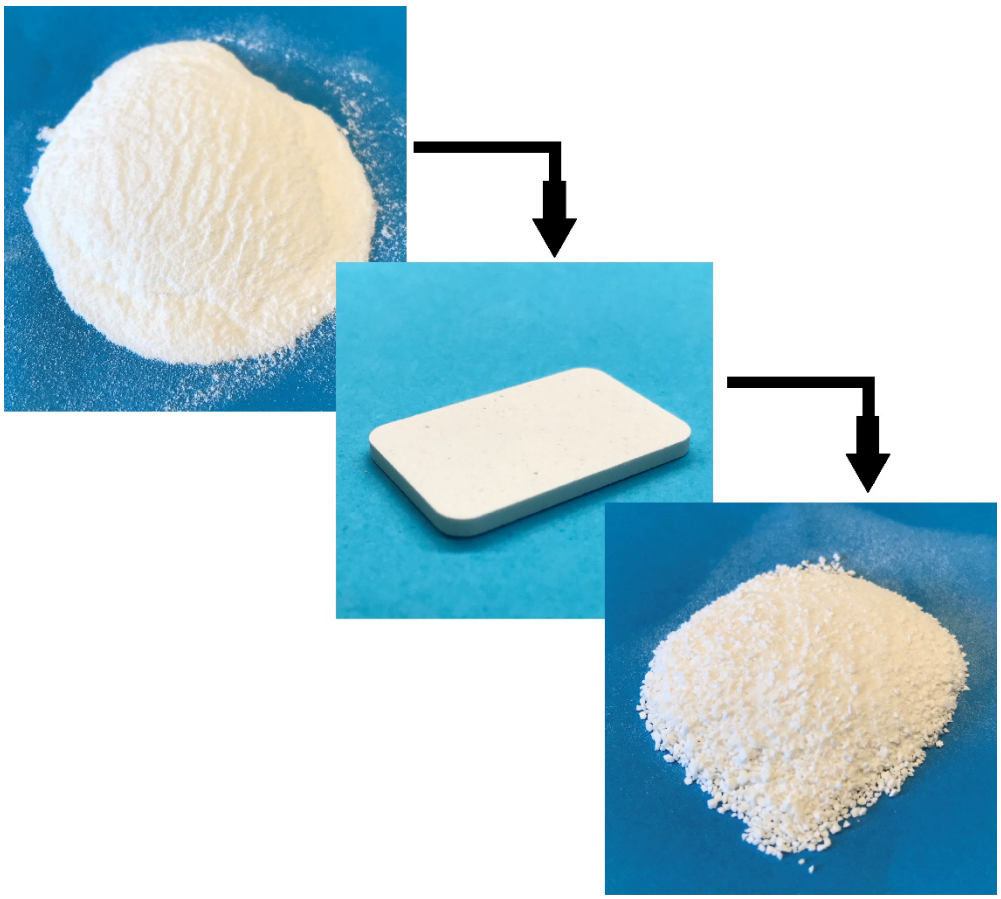

By Mathias Bjerring Olesen, 31st of May 2022

Abstract

Novo Nordisk search for a way to make their near-infrared (NIR) methods for protein assay in granulate methods robust without having to use enormous amounts of resources in production of samples to be used for calibration models. A downscaled dry granulation process was developed and it was demonstrated how NIR spectroscopy can be used for evaluation and assessment during development. The aim was to be able to control three different attributes in the granulate: BSA concentration, particle size and water content. The project was successful in developing such a process. That process was then used to produce a sample set. As proof-of-concept, regression models were calibrated on NIR measurements of the sample set that were then subsequently challenged in a robustness study.

Acknowledgements

I would like to thank my supervisors, Erik Skibsted (Principal Scientist, Novo Nordisk), Niels Peter Aae Christensen (Senior Formulation Scientist, Novo Nordisk), Franciscus Winfried J van der Berg (Associate Professor, UCPH) and Rasmus Bro (Full professor, UCPH).

Thanks to the rest of team 6908.02 Real Time Release Testing for helping with various bigger and smaller tasks, whether it being laboratory-related, helping with MATLAB code or sparring in general.

Table of Contents

Introduction

A dry-granulation process is a common practise in production of tablets for oral medication. There are several advantages of such a process. One being that the homogeneity state of the initial ingredients is stabilized in crystal structures in granulate (Bhavishya Mittal, 2017). This is advantageous as providing the right dosage of API becomes easier. A high degree of quality needs to be maintained and documented to ensure patient safety and compliance with demands from the regulatory authorities. Lately, process analytical technology (PAT) has been acknowledged in the pharmaceutical industry (Reich G., 2005), (FDA, 2004) and (Higgins JP. et al., 2003). PAT can help ensure and document quality in a process such as dry granulation. An often used PAT technology is NIR spectroscopy that coupled with chemometric techniques can be used to calibrate a model for monitoring API concentration. A prerequisite for calibration of such a model is a sample set the contains sufficient variance. Using production samples limits the robustness of such a calibration as the chemometrician has little access to samples with variance. Running a production is too expensive for the sole purpose of producing samples with varying qualities.

Project motivation and description

A team at Novo Nordisk develops and provides NIR methods to quantify protein in different matrices, both off-line in separate laboratories and in-line within the production equipment. One such method is an off-line protein assay of granulate through bottom of glass NIR vials. Problems of bias in protein predictions has been observed. The current strategy to solve this problem is to use a larger dataset. However, as described earlier, getting the right kind of samples is expensive and time consuming. The current hypothesis is that both water and particle size variances result in new and unexplored variation in the sample matrix.

This project will aim at designing a down-scaled dry granulation process where particle size and water content is controllable in the final granules. Furthermore, as proof-of-concept, the process will be used to produce a large sample set that, measured with NIR, will form a dataset to be used in an attempt to calibrate a robust NIR model for protein assay prediction.

Theory

Dry-granulation process

In the dry-granulation process there are three physical phases for the product material: powder, solid and granulate. After powder ingredients have been homogenized, the mixture is fed into a roller compactor that compact the powder together such that it forms a solid ribbon (see Figure 1).

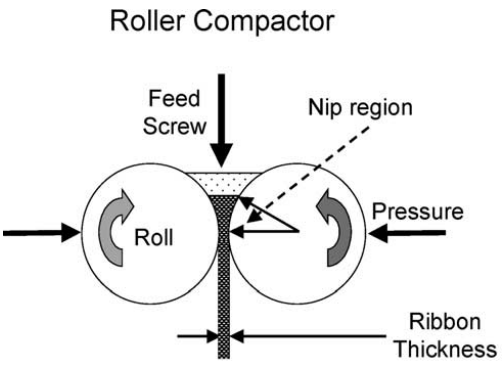

Figure 1: Sketch of the roller compaction process (Zinchuk et al., 2003).

An active roller compaction process at a research facility at Novo Nordisk was observed during this project. The operators and scientists had different parameters they could adjust until the process ran smoothly. A fixed pressure was set for the rollers to maintain throughout the process. An operation optimum as well as specification limits of a gap-size between rollers in the compression (nip) region was set to achieve ribbons of a specified thickness. The gap-size depended on feed velocity and pressure and would increase or shrink accordingly. Therefore, the main adjustments were related to the rotation speed of a screw that controlled the feed velocity.

The ribbons will fall down into a shredding unit to be crushed, shredded and sifted to form the final granulate.

NIR spectroscopy

Near infrared (NIR) spectroscopy is a non-destructive analysis method that can be used to analyse chemical and physical product properties in granulate (F. Shikata et al., 2017). The measurements takes little time and effort to perform which is why NIR is often used for real time process monitoring. NIR operates using the unique ways that molecules interacts with light in the region 12500-4000 cm^{-1} in the electromagnetic spectrum. These interactions happens when light is absorbed or emitted and cause changes in vibrational energy in molecular bonds. An electromagnetic wave carries energy that is specific for its' frequency. Any unique constellation of atoms within a molecule will result in a specific vibration in a chemical bond. If a vibration has affinity to the frequency of an electromagnetic wave, the wave, as well as its overtones, can get absorbed. The primary spectral features seen in the NIR absorbance spectrum is due to overtones and combination bands. For granulate, this absorption can be detected through reflectance NIR spectroscopy. Several diffuse reflectance NIR equipment systems were used during this project.

Pre-processing

The NIR absorption spectrum most often needs some amount of spectrum pre-processing whose purpose is to reduce random noise and systematic variations and to enhance properties of interest in the spectrum. Such reductions are highly relevant when measuring granulate as the varying particle

sizes cause light scattering effects (Hu Changqin et al., 2010). The pre-processing techniques used during this project are Mean Centring (MC), Autoscaling, Standard Normal Variate (SNV), Multiplicative Scatter Correction (MSC), Extended Multiplicative Signal Correction (EMSC) and Savitzky-Golay 1st and 2nd derivative (Roger JM., 2020).

Method and Discussion

Down-scaling the dry granulation process

The initial investigations on the different aspects of the dry granulation process uses a powder blend of 98% microcrystalline cellulose (MCC) and 2% magnesium stearate (MgSt). Later, the API substitute Bovine Serum Albumin (BSA) will be incorporated in the investigations. The powder was blended for 45 minutes with a 20 rpm rotation speed in a SentroBlender (Sentronic, Dresden, Germany) using a 250 mL Duma container as mixing vessel. The blending process was investigated in a previous project (Olesen M., 2022).

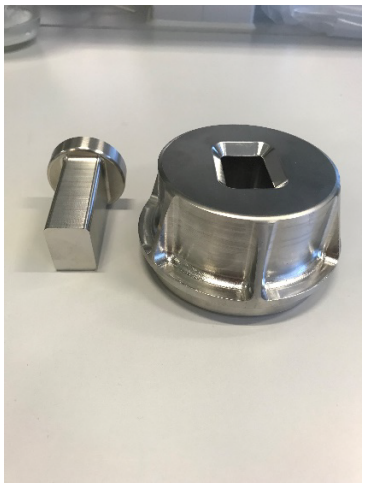

Figure 2: Custom designed piston die for pressing riblets.

Figure 3: Hydraulic press with custom designed piston die.

Making the riblets

To imitate the production of ribbons through compaction in a production setting, a setup was designed using a custom designed piston die fitted to an Atlas Manual Hydraulic Press 15T (Specac, Orpington, United Kingdom) as seen on Figure 2 and Figure 3.

It was decided to use 1.5 g of a powder blend consisting of MCC and MgSt for compaction of smaller rectangular, surrogate ribbons called a riblet. The powder was weighed using a DeltaRange XS4002S scale (Mettler Toledo, Greifensee, Switzerland) and transferred to the piston die. The piston die was placed in the hydraulic press and a pressure was applied thereby compacting the powder into a solid riblet (see Figure 4).

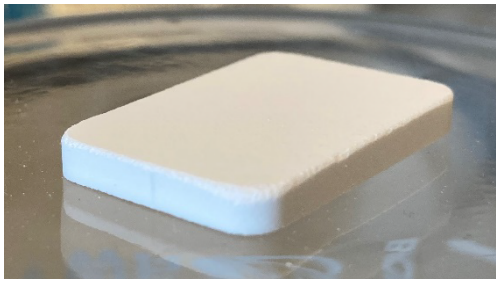

Figure 4: The resulting riblet after compaction in the hydraulic press. This riblet was compressed using 84.3 kg_f/cm^2.

Pressure effect on riblet solid fraction

One key attribute of riblets is their solid fraction, SF. The SF is proportional to the envelope density, ρ_e, and has a linear relationship with the porosity, P, of the riblet:

$$SF = \frac{\rho_e}{\rho_t} = \frac{100 - P}{100}$$

Where ρ_t is the true density or maximum density of a material.

The SF delivers information about mechanical properties of the riblets. It indicates the degree to which the material has been compacted which impacts e.g. tensile strength (Gregory et al., 2009).

Zinchuk et al., 2003, simulated a roller compaction process of MCC in a laboratory environment and evaluated the produced ribbons on their SFs and tensile strengths. One of their investigations was on the relationship between the pressure delivered on the powder and the ribbon SF. They found that a pressure between 10 and 45 kg_f/cm^2 resulted in ribbon SFs between 0.48 and 0.72. In the setup used for this thesis, the riblet top-side area is 5,93 cm^2. To match that investigation in this project, a pressure range of 0.080 and 0.25 tonnes was applied with the hydraulic press when making the riblets. After compression, the riblet thickness was measured with a digital caliper. The riblets that were produced within the pressure range gave SFs between 0.34 and 0.48. The SFs differs from those found by Zinchuk et al., 2003. This might be due to them using a continuous roller compaction simulating setup while the setup used in this project is batch based. Also, the riblets are thicker than the ribbons produced by Zinchuk et al., 2003. A broader pressure range was used going from 0.080 to 10 tonnes, corresponding to 13 to 1685 kg_f/cm^2. This range practically spans the entire compaction range as evident in Figure 5. The SFs asymptotically approaches 1 when the weight for compaction of the riblets is increased. The physical appearance changes quite a bit as can be seen on Figure 6. The least compacted riblet barely holds together whereas the most compacted riblet is smooth as a kitchen tile and hard.

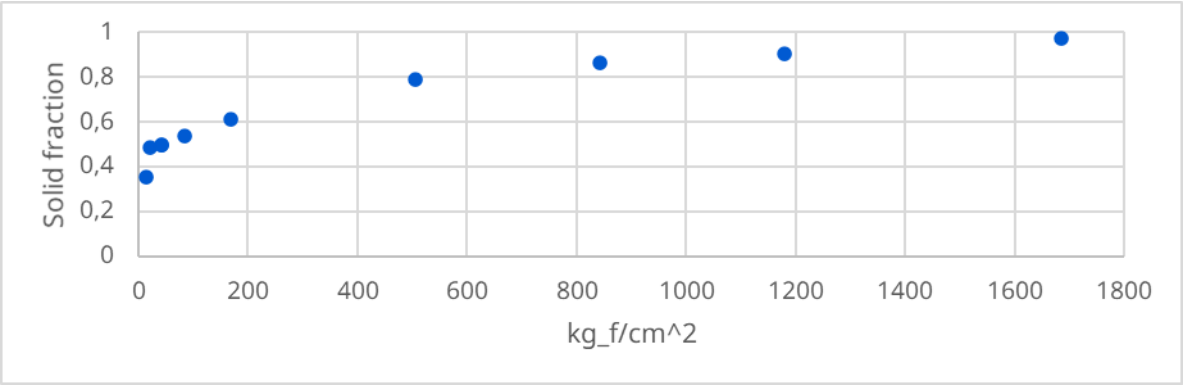

Figure 5: Solid fraction of riblets compacted under different pressures.

Figure 6: Examples of riblets compacted under different pressures.

Riblet solid fraction prediction with NIR

A small experiment was set up to build a model to predict SF using NIR. The roller compactors used at Novo Nordisk are variants of PACTOR® roller compactors (Gerteis, Jona, Switzerland) to which an in-line NIR probe equipment such as a SentroProbe (Sentronic GmbH, Dresden, Germany) could be fitted for real time SF measurements of ribbons. Three different spots on the riblets were measured with a SentroProbe as shown on Figure 7 to produce NIR spectra. The NIR spectra were used for calibration and validation of SF prediction models according to Table 1. Each spot was measured multiple times to produce 157 and 43 measurements for calibration and validation, respectively. The calibration data set is visualised in Figure 8. The tendency is that the higher the compaction weight, the higher the absorbance. The riblets compacted with 0.125, 0.25 and 0.5 tonnes gives raw spectra that are indistinguishable from each other with the naked eye. But there seems to be a nonlinear tendency in the data set as evident in Figure 9 where a scatter plot of the intensity of each measurement at 2000 nm against the riblet solid fraction can be seen. The spectra were pre-processed with SNV and MC and a PCA model was calculated. A PCA scores plot can be seen in Figure 10. PC1 explains SF variance in the riblets. For 5 out of 7 of the riblet classes, three distinct groups are visible, one for each spot measured on a riblet. They are mostly separated by PC2. The riblets were measured twice on one side and once on the other. Therefore, PC2 could explain the difference between the two sides of the riblet.

Figure 7: NIR measurement of a riblet using the SentroProbe.

Table 1: Overview of the nine riblets that were measured for calibration and validation of a SF prediction model.

Pressure used during riblet compression $[kg_f/cm^2]$	Corresponding compression weight [T]	Used for calibration data set	Used for validation test set
21.2	0.125	x	
42.1	0.25	x	
42.1	0.25		x

Table 1: Overview of the nine riblets that were measured for calibration and validation of a SF prediction model.

Pressure used during riblet compression $[kg_f/cm^2]$	Corresponding compression weight [T]	Used for calibration data set	Used for validation test set
84.3	0.5	x	
169	1	x	
506	3	x	
843	5	x	
1180	7		x
1685	10	x	

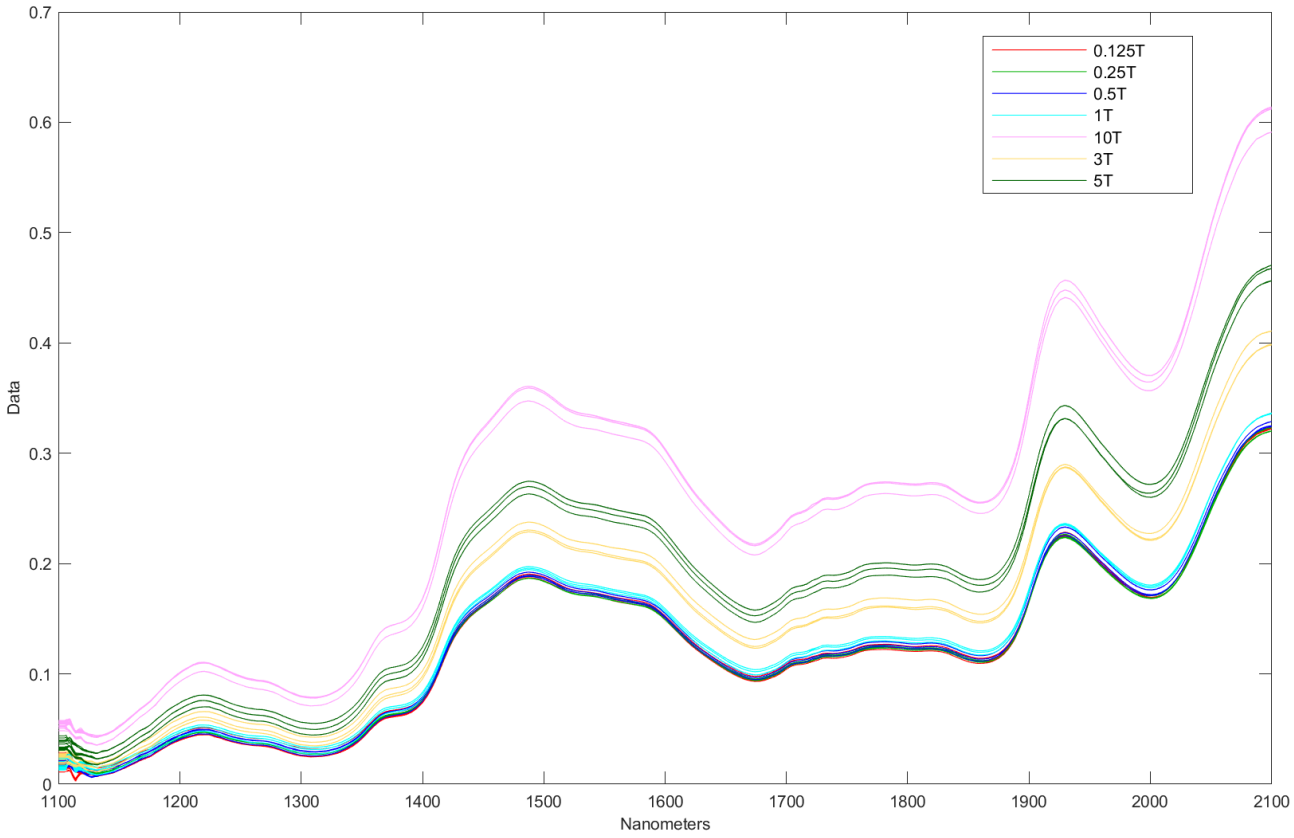

Figure 8: Raw NIR spectra measured on the riblets used for calibration data set. The Y-axis measures absorbance.

Two SF prediction models, PLS and SVM, were calibrated. SNV and Mean Centring were used as pre-processing methods. A custom method was used for cross-validation where each subset consisted of measurements from the same riblet. SVM was tried to see if it would perform better than PLS with the nonlinear data. The models performances can be seen in Figure 11 and Figure 12. Judging from the RMSE metrics, SVM does not perform better than the PLS model. However, when inspecting the

residuals plots in Figure 13 and Figure 14, it can be seen that grouping of measurements taken on the same spot on a riblet is apparent in both Figure 10 and in the residuals plot for the SVM model. This indicates that there is SF variation within a riblet which is to be expected as uneven powder distribution can occur when filling the piston die. This inter-riblet SF variation is not measurable with a caliper, meaning that some systematic error is introduced into the calibration models. If this systematic error was mitigated, the SVM model would likely perform better than the PLS model. Going forward, the step regarding filling of the piston die will be handled more carefully to ensure even distribution of powder.

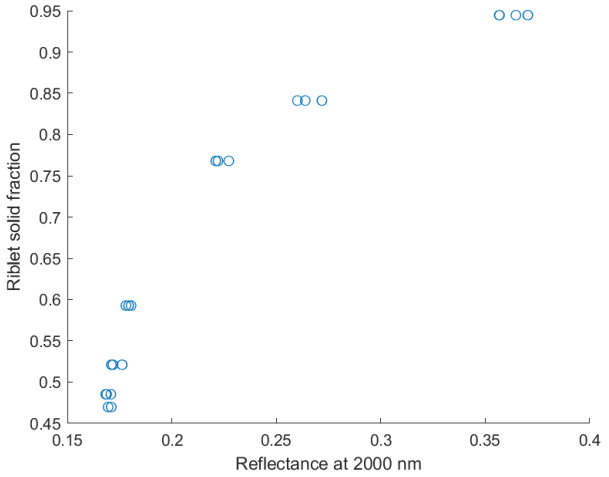

Figure 9: Riblet SF vs. reflectance at 2000 nm for the riblets used for the calibration data set.

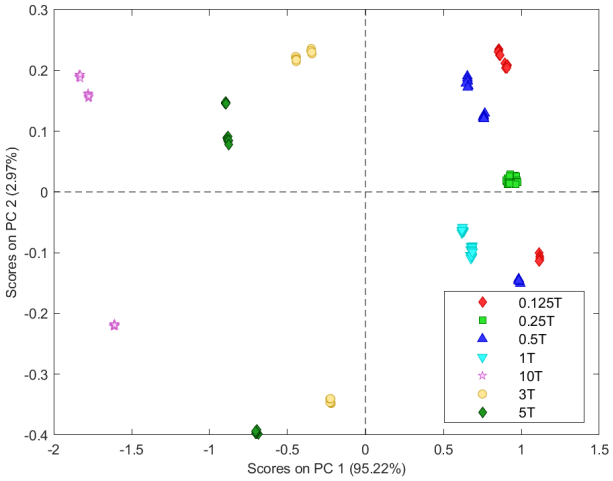

Figure 10: PC1/PC2 scores plot of the PCA model using the calibration data set with SNV and MC as pre-processing.

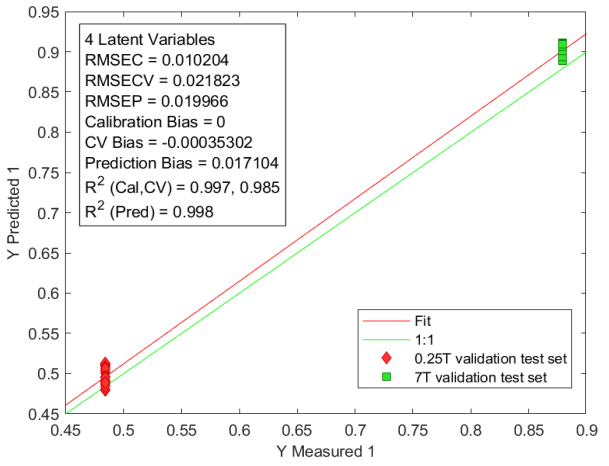

Figure 11: Riblet SF prediction model using PLS including model information and validation test set.

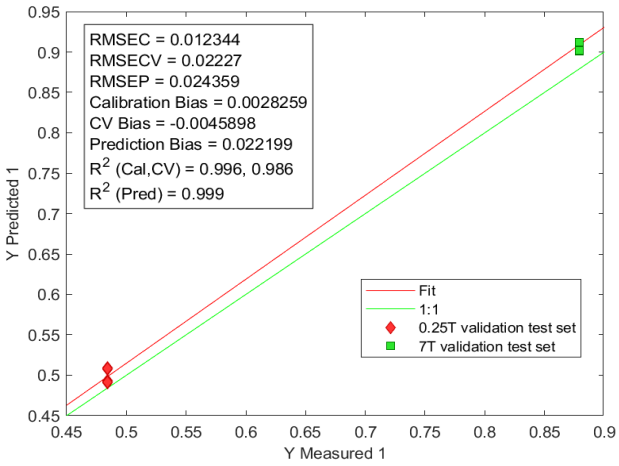

Figure 12: Riblet SF prediction model using SVM including model information and validation test set.

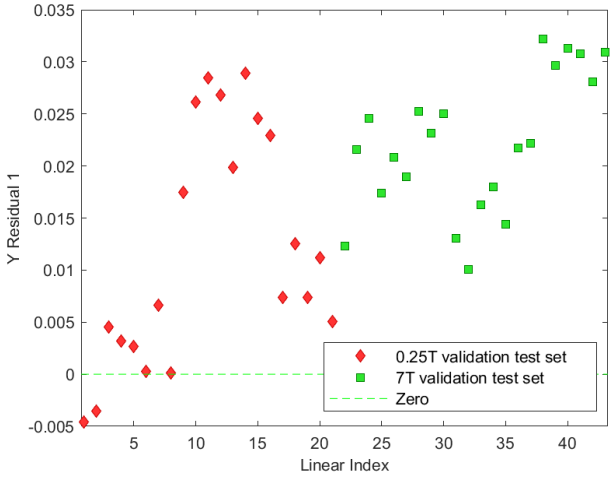

Figure 13: Residuals when using the PLS model to predict SF on the validation test set.

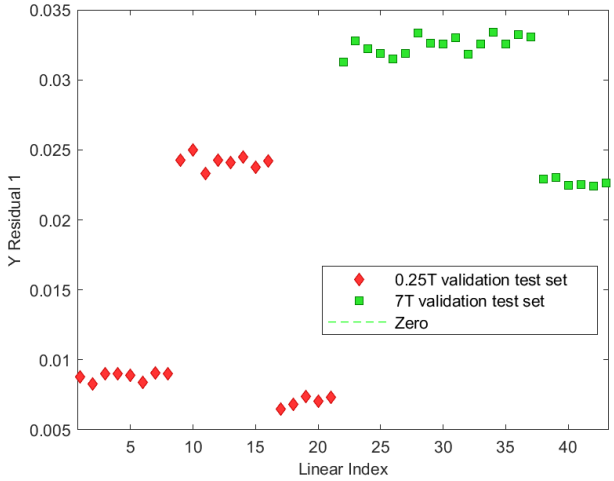

Figure 14: Residuals when using the SVM model to predict SF on the validation test set.

This investigation on riblet SF has given knowledge on how the compaction step impacts the riblets and what pressure to use to achieve a certain SF. SF can be predicted using NIR and the modelling using NIR measurements has given insight into what variance is introduced by the compaction process.

Making the granulate

To imitate the production of granulate in a production setting, the riblets from the compaction step were shredded in a Small Scale Mill (Gerteis, Jona, Switzerland) (see Figure 15).

Table 2: Overview of the different riblet batches produced to investigate the granulation process.

Riblet weight [g]	Compression weight [t]	Batch number
1.5	0.125	1
0.5	3	4
1	3	5
1.5	3	2
1	6	6
1.5	6	7
1	10	8
1.5	10	3

Figure 15: Small Scale Mill from Gerteis.

Eight batches of riblets were produced for which the attributes can be seen in Table 2. Each batch aimed for a total of 30 g of material before shredding. Inside the mill was a 0.8 mm conidur screen that would shred the riblets when pushing and pulling the lever on top. Some loss in material was noticed, especially for the riblet batches using 1.5 g of material and for riblet batches using lower compaction weight, as the material would clog the screen. For this granulation investigation, the screen was dusted off between batch runs. The powder blend and some of the resulting granulate can

be seen in Figure 16, Figure 17, Figure 18 and Figure 19. The granulate produced from batch 1 in Table 2 does not differ visibly from the powder blend but the granulation becomes more distinct when the compaction weight is increased in batch 2 and batch 3. Batches 4, 5, 6, 7 and 8 were produced after the three others to investigate further, e.g. the effect of riblet thickness on the granulation.

Figure 16: Powder blend before compaction

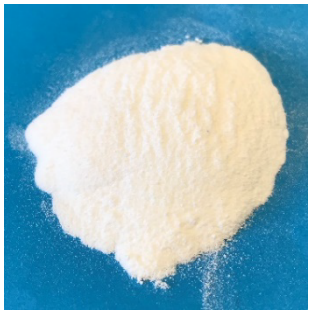

Figure 17: Granules from batch 1 in Table 2.

Figure 18: Granules from batch 2 in Table 2

Figure 19: Granules from batch 3 in Table 2

Mass reduction and granule measurements

The granulate batches yield-masses were a little less than 30 g. For this investigation, it is not feasible to have such big samples while trying to get representative measurements. Also, replicate aliquots of each granule batch is needed in the following investigations. Therefore, a mass reduction sampling method was used to divide the granulate batches into smaller aliquots. The chosen method was adapted from a method described by Gerlach et al (2002) and used an A3 paper folded into a cone with eight riffles as seen on Figure 20(a). One collection container was placed under each riffle and the granulate sample was poured onto the paper cone riffle splitter in a circular motion using a beaker and a funnel as seen on Figure 20(b). Multiple rotations were completed with a uniform rotation speed while the material was dispensed. Some loss of material was noticed during this operation. A small fraction of the larger particles tended to jump around and miss the collection containers and a small fraction of the smaller particles tended to stick to the paper. The eight aliquots of material per batch were transferred into NIR vials. At this point an average of 4.28 g material was lost during granulation and mass reduction. The eight aliquots in NIR vials for each of the eight batches were measured through the bottom of the vial with an MPA-II FT-NIR Multi-Purpose Analyzer (Bruker, Ballerica, MA, USA) using an integrating sphere NIR reflectance module. Each measurement used a resolution of 8 cm^{-1} and 32 scans in the range from 11550 cm^{-1} to 3950 cm^{-1}.

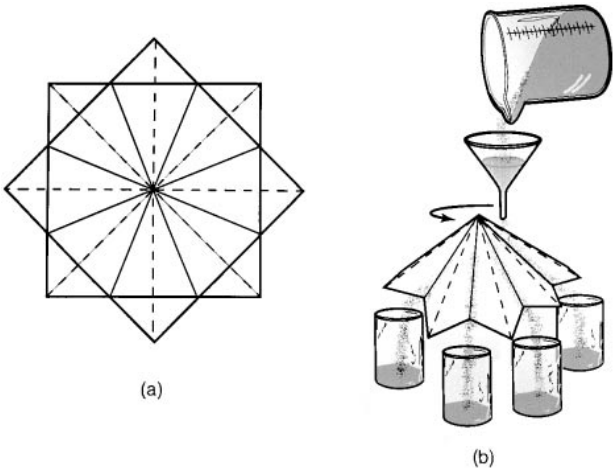

Figure 20: Paper cone riffle splitter. (a) This template for a paper cone riffle splitter is based on two 30 cm squares, one rotated 45 ° with respect to the other. (b) The sample is poured through a funnel rotated around the centre of the paper cone. (Gerlach et al, 2002).

Investigating the riblet quality's effect on granulation

The granule batches 1-3 in Table 2 were measured 8 to 10 times per vial. The vials were picked up, turned and rotated in between measurements. The spectra can be seen in Figure 21. There is much light scattering present and it is evident that the granulates made from riblets that were compacted using 10 tonnes of pressure results in the highest absorbance. The spectra were pre-processed with EMSC and MC. A PCA model was calculated and the scores plot can be seen in Figure 22. 24 outliers were removed and investigations found that:

1. The vials need to be rotated and turned before measuring. Otherwise, they could result in outlier measurements.
2. The NIR vial fittings on the equipment's auto-sampler need to be inspected to ensure that they are not loose. The distance to the integrating sphere can vary if the fittings are loose and will result in an outlier measurement.

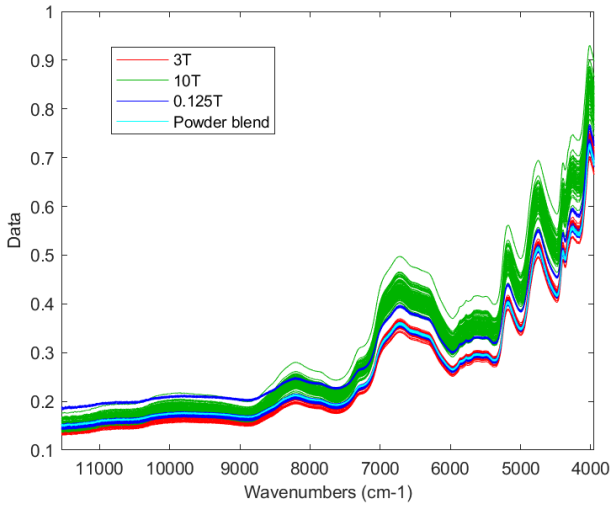

Figure 21: NIR spectra of the powder blend and of the granulate made from batches 1-3 in Table 2.

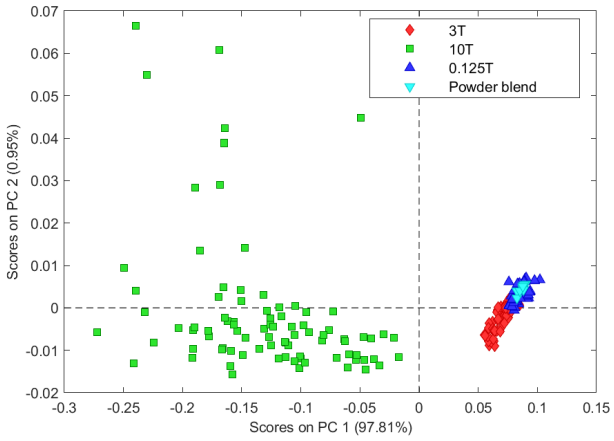

Figure 22: Calculated PCA scores plot of the EMSC and Mean Center pre-processed data presented in Figure 21. 24 outliers has been removed.

From Figure 22 it can be seen that the riblets compacted using different amounts of weight forms groups that are mostly separated by PC1. Riblets compacted using 0.125 tonnes produces granulate that is indistinguishable from the powder blend. It indicates that the riblets are separated into primary particles after shredding which was also noticed earlier upon visual inspection of the granulates. The riblets compressed using 3 and 10 tonnes produces granulates that separates themselves from the powder blend both visibly and when measuring it with NIR. The measurements of the granulate produced from the riblets compacted using 3 tonnes are relatively tightly clustered, whereas, for the granulate made from riblets that were compacted using 10 tonnes, the measurements gives a relatively high spread for the group. This could be because the granulate particle size produced from the riblets compressed using 10 tonnes is larger or the distribution in particle size is wider making it more difficult to produce a representative measurement. It seems that there is also some non-linearity in

the data which fits with what was previously discovered about SF and non-linearity in relation with NIR absorbance.

A further inspection into the grouping of measurements on the granulate produced from the 3T compressed riblets show that the mass reduction sampling method is not completely representative (see Figure 23). Each vial creates a grouping within the 3T group. The granulate in vial 4, 5, 6 and 7 stems from adjacent aliquots from the aliquotation and they tend to produce higher scores on both PC1 and PC2. This suggests that there is introduced systematic error from the aliqoutation. However, the vial groupings overlap and the sampling method was deemed acceptable for this project. Going forward, each vial will be measured 3 times only.

One aim of the downscaled granulation process is to produce batches of granulate with different particle size characteristics. This aim seems to be achievable by controlling the SF of the riblets. However, the production scale granulation process uses ribbons with relatively constant SF. Zinchuk et al., 2003, found that ribbons of acceptable quality had a SF range of 0.57 to 0.80 with a mean of 0.70. The riblets compacted using 0.125 tonnes has a SF of 0.47, for 3 tonnes it is 0.77 and for 10 tonnes it is 0.94. Only the riblets compacted with 3 tonnes results in an acceptable SF.

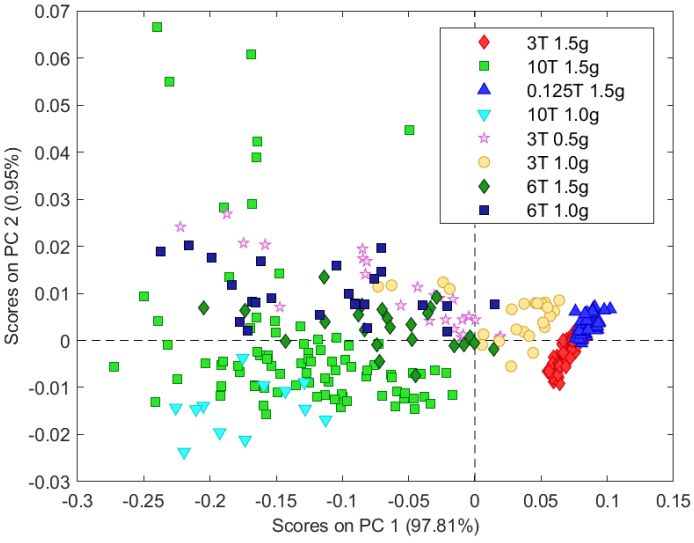

Figure 26: PCA scores for NIR measurements of granulate made from batches 1-8 in Table 2 predicted from the PCA model calculated for Figure 22.

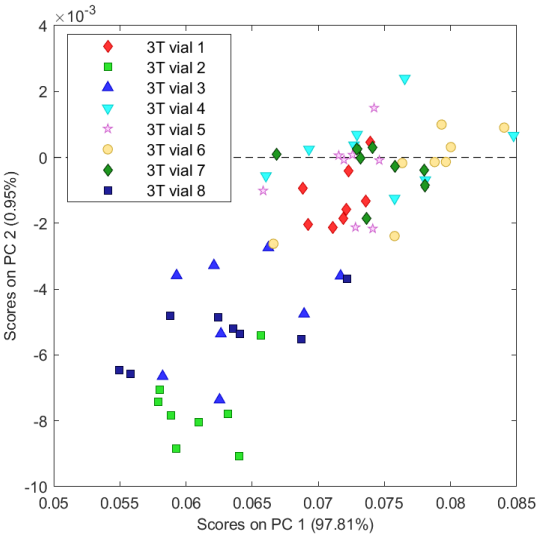

Figure 23: Zoom-in on the 3T grouping in Figure 22 and coloured according to vial number. The other groupings in Figure 22 has been removed here.

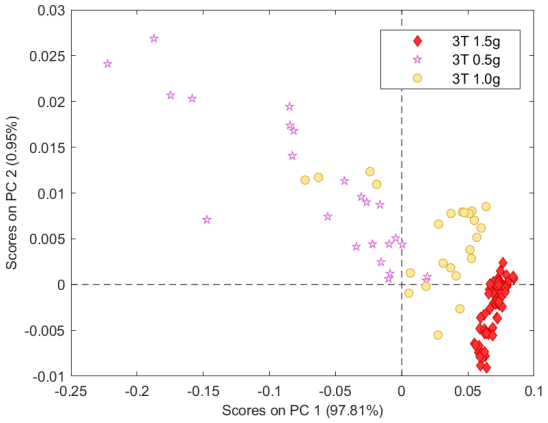

Figure 24: Isolated PCA scores of the 3T fractions from Figure 25.

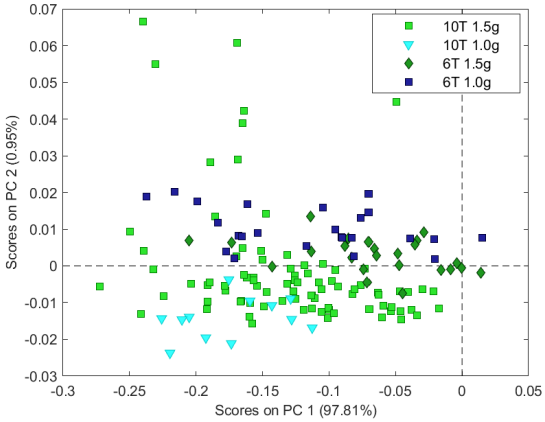

Figure 25: Isolated PCA scores of the 6T and 10T fractions from Figure 25.

The riblet batches 4 to 8 in Table 2 were produced to investigate the effect of riblet thickness on the granulate characteristics. The riblet thickness was controlled by the amount of powder blend material used in the piston die during compaction. The riblets were shredded into granulate and measured with NIR. The PCA scores for granulate NIR measurements on batches 1-8 were predicted using the calculated PCA model (see Figure 25, Figure 24 and Figure 26). Batch 8 did not yield the 30 g of riblets as was the case with the other batches. The reason for this is that the piston die got jammed because of the high pressure used for this fraction. Looking at the PCA scores, there is a tendency that the thicker the riblet, the higher the score on PC1 and the narrower the spread in the scores. This is mostly noticeable when looking at the 3T fractions in Figure 24. Also, the non-linearity that was previously associated with different SFs seems to be absent when looking at the 3T fractions. The SF for the 0.5 g, 1.0 g and 1.5 g 3T fractions were 0.71, 0.76 and 0.77, respectively, whereas the SF for the 6T and 10T fractions were 0.87 and 0.93-0.94, respectively.

From this investigation it was found that the granulate particle characteristics can be controlled by the amount of powder blend material used for compaction of a riblet. Other ways of controlling the granulate particle characteristics is by changing the SF of the riblets and possibly changing the conidur screen mesh size. However, these two ways would not be representative for the production scale granulation process. In the production scale process, the conidur screen mesh size is pretty much a standard across the dry granulation processes in Novo Nordisk and the SF is within the specifications demanded by e.g. the tabletting process. When the production scale granulation process is running, a compaction pressure is defined that is then held constant through the roller compaction process. An aim of a specific gap size between the wheels in the roller compacter is defined. The primary parameter to be adjusted is the flow speed of powder. The flow speed has an impact on the gap size. Therefore, the flow speed is adjusted until the gap size is stable. This operation of adjusting the flow speed in the production scale dry granulation process is relatable to adjusting the amount of material used during compaction of the riblets in the small scale batchwise process developed in this project. Therefore, it was decided to use a weight of 3 tonnes when compacting the riblets going forward. One concern regarding the chosen fraction of 0.5 g riblets is that the thickness of the riblet is close to the conidur screen mesh size. This could result in granulate made entirely of small discs and create a different type of granulate characteristic. This could have an unwanted effect on the NIR calibration model for predicting API concentration. This effect is investigated further in the API processability study where batches of riblets from a larger range of riblet thicknesses are included.

API processability study

Up until now, the investigations have included placebo formulations containing only MCC and MgSt. Some of the processes (e.g. blending, compaction and granulation) could be affected by addition of the model API protein, BSA, to the formulation. The following API processability study will confirm that the learnings from the previous investigations also holds when BSA is added.

Blending

A previous project investigated the blending process. The project used in-line NIR to track the blending of MCC and MgSt. The project aim was to find an optimum within the parameters; rotation speed, fill percentage in mixing vessel and MgSt concentration. The project ended up suggesting 20 rpm and 60 % fill percentage and blending for 45 minutes. Using this suggested rotation speed and fill percentage would ensure a fully mixed powder blend after 45 minutes. One method of assessment used in the previous project was a PLS model that was calibrated on the in-line NIR measurements to predict MgSt concentration. That model cannot be used to assess the blending where BSA is included. Therefore, a PCA model of a blending using the placebo formulation with 20 rpm rotation speed, 60 % fill volume and 45 minutes blend time will be compared with one where the formulation includes BSA. Both formulations used 2 % MgSt concentration which is similar to what could be used in a dry granulation production scale process at Novo Nordisk.

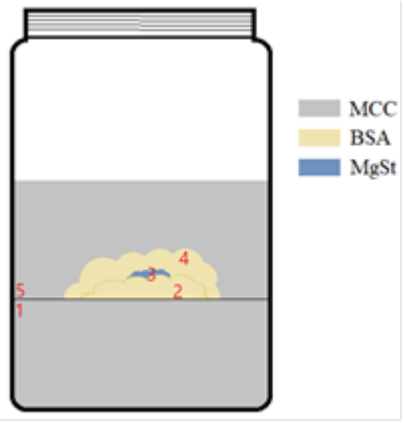

Figure 27: A sketch of how a 250 mL duma was filled before mixing. 1, 2, 3, 4 and 5 indicates the order of which the powder was added to the container.

The BSA that was acquired had been spray dried and consisted of larger crystals of several millimetres in size. The crystals were grinded using a mortar and a pestle and sifted using a 250 micron mesh. Because the density of the three powders are different, the powders density were measured using a duma of known volume and the lab scale. This was mainly done to ensure that the fill volume of 60 % was met at the beginning of mixing. A 250 mL duma container was filled with 88 % MCC, 10 % BSA and 2 % MgSt such that the MgSt was centred and enveloped with BSA that yet again was enveloped with MCC as sketched in Figure 27. The container was positioned in a SentroBlender (Sentronic, Dresden, Germany) with a SentroPAT in-line NIR equipment (Sentronic, Dresden, Germany) attached. The SentroBlender is a rotary blender that can fixate a container such that the container opening is pushed onto a glass window through which the NIR equipment can measure once every rotation (see Figure 28). The NIR spectra measured by the SentroPAT is in the range 1350 nm to 1800 nm.

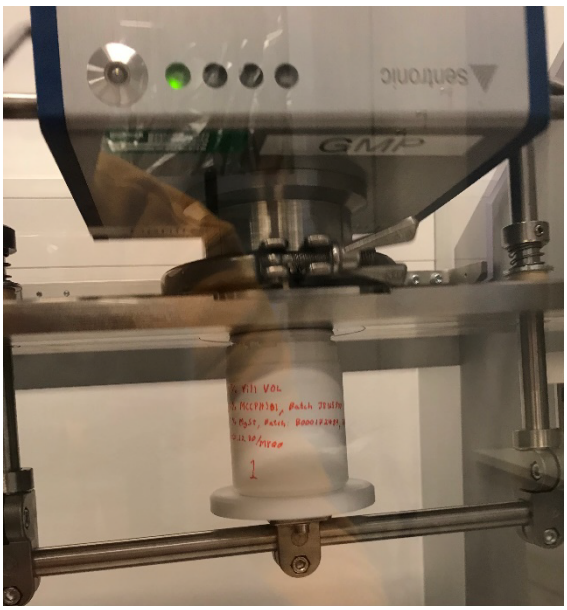

Figure 28: Example of the blending setup and how the SentroPAT equipment measures into the Duma container.

A PCA model was calculated for each of the two blends using SNV and MC as pre-processing. The respective loadings and scores plots are compared to see if similar patterns can be recognised (see Figure 30, Figure 31, Figure 32 and Figure 33). The two models are quite similar. PC 1 describes a physical change in the powder during mixing associated with MCC. In the previous

project that investigated the blending process it was found that this loading was also present when mixing a 100 % MCC formulation. The PC1 loading for the BSA blend model does differ from the placebo blend model in the information described between 1700 and 1750 nm. This is also the area where both BSA and MgSt has most absorption in the recorded NIR spectrum. Figure 29 shows the NIR spectra of the three pure ingredients. When comparing the pure spectra with the loadings for each of the two models, it can be seen that the loading for PC2 for the placebo blend model is highly associated with MgSt (see Figure 32). The loading for PC2 for the BSA blend model is also but not as highly associated with MgSt (see Figure 33). This could be because MgSt and BSA both have their highest absorption in this part of the recorded NIR spectrum.

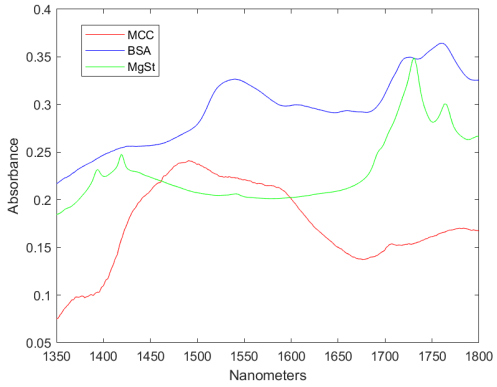

Figure 29: NIR spectra of pure MCC, BSA and MgSt.

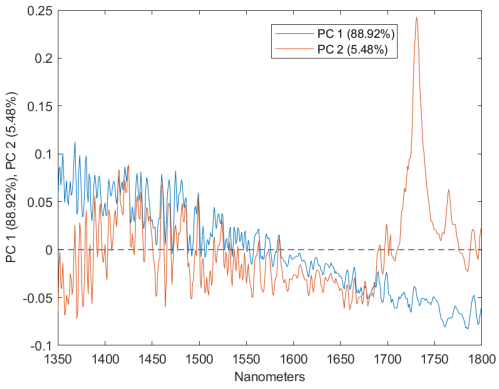

Figure 32: PCA loadings plot incl. PC1 and PC2 for the placebo formulation blending.

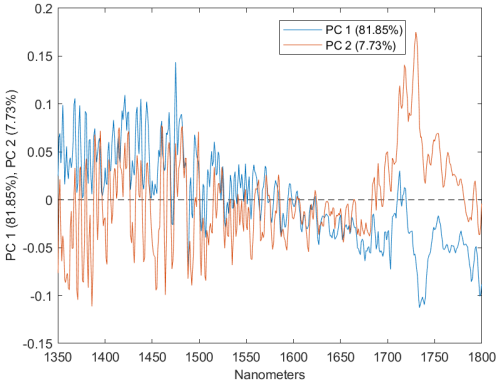

Figure 33: PCA loadings plot incl. PC1 and PC2 for the BSA formulation blending.

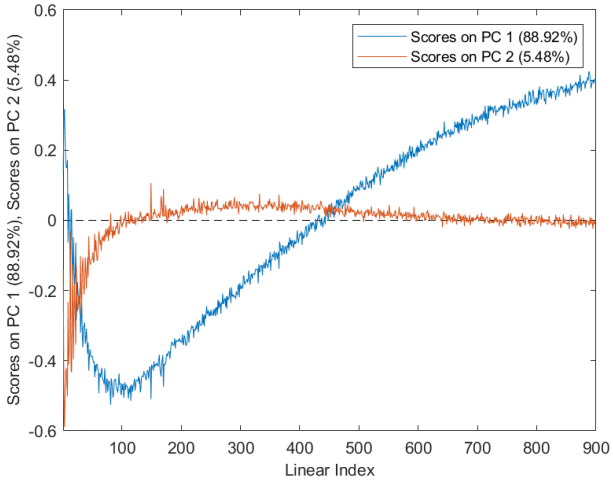

Figure 30: PCA scores plot incl. scores on PC1 and PC2 for the placebo formulation blending.

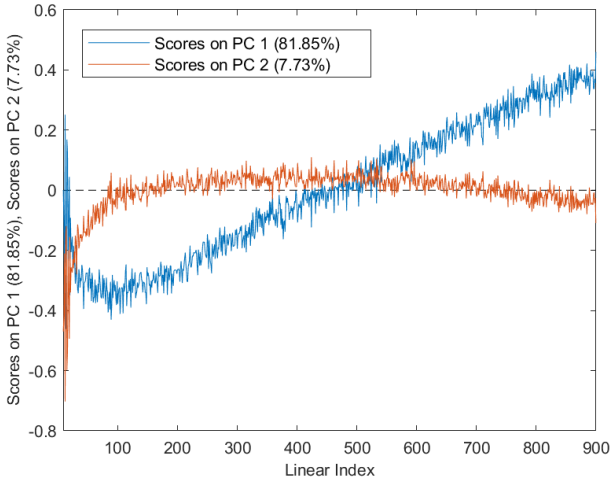

Figure 31: PCA scores plot incl. scores on PC1 and PC2 for the BSA formulation blending.

A comparison between the blending of the placebo formulation and the BSA formulation can be made by comparing the change in scores on PC1 and PC2 during blending (see Figure 30 and Figure 31). The scores on PC1 and PC2 for the BSA formulation blending are more noisy. This could be caused by the BSA particles that most likely are bigger and less uniform compared to MCC and MgSt. However, judging from the scores, it seems that the two formulations follows a similar blending behaviour. This is the rationale used to support using the blending settings of 20 rpm, 60 % fill volume in duma and 45 minutes blend time as suggested by the previous project on the blending process will work for a formulation that includes BSA.

Compaction and granulation

A study was made on the compaction and granulation steps to determine if the BSA formulation would show the same behaviour as the placebo formulation. Also, the effect of powder mass used during compaction on the granulate characteristics was investigated further by using batches of riblets with 10 % BSA concentration and masses: 0.5 g, 1.0 g, 1.5 g, 2.0 g and 2.5 g. The resulting SFs after pressing these riblets were between 0.80 and 0.82. This is on the limit of being too high according to the range identified by Zinchuk et al., 2003. However, the calculations are dependent on the accuracy of the caliper method and, as has been noticed earlier, the riblets contain inter-riblet SF variation. For this project, it is sufficient with these SFs as there yet are no specifications for the granulate. Future work could try and optimize the compaction step to achieve a desirable SF in the riblets that corresponds to the ribbons produced at the local production facilities.

The riblet batches were grinded, divided into aliquots in NIR vials and measured with NIR as described earlier (see section Mass reduction and granule measurements) with one change being that, instead of a 8 pointed star paper riffle splitter, a 12 pointed star paper riffle splitter was used. This change was implemented as four sets of triplicates within each granulate batch was desirable for future processes. There was a risk that this change will have an effect on the representativeness of each aliquot. A PCA model was calculated using the earlier NIR measurements of the granulate from placebo formulation riblets compacted using 3 tonnes and the BSA formulation granulate produced in this API processability study. The NIR spectra were pre-processed using EMSC and MC. Three outlier measurements were excluded. The PCA scores plot in Figure 34 shows that there is a tendency of variance in the NIR spectra caused by varying riblet

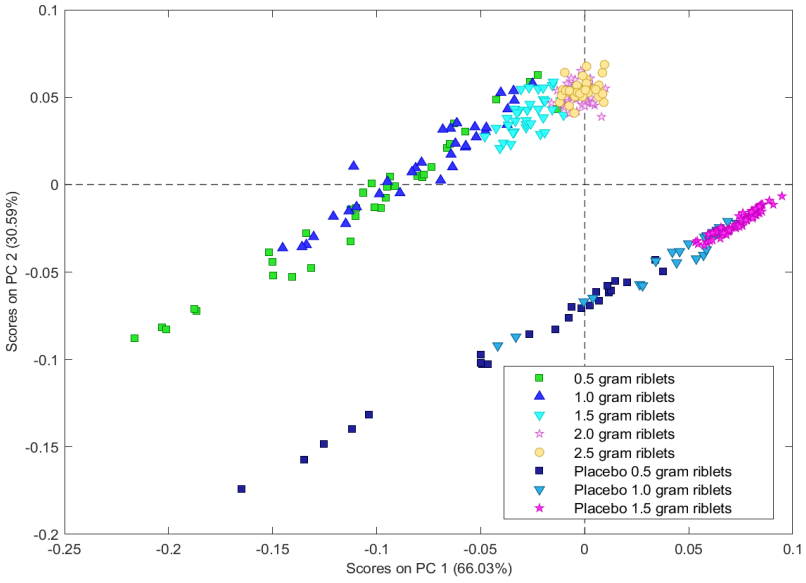

Figure 34: PCA scores plot of 10 % BSA granulate batches and placebo batches with the batches differing and coloured by the mass used for the riblets.

masses in both the placebo formulation granulate and the BSA formulation granulate. The two formulations are also separated as a result of present and absent BSA signal. Another thing that is noticeable is that the BSA granulate measurements produces a cloud of scores that also separates in the same direction that separates the two formulations. The placebo formulation does not show this effect to the same degree. Looking at the BSA formulation granulate, the 2.0 and the 2.5 gram riblets granulates produces similar scores. For both the placebo formulation and the BSA formulation, the 0.5 gram riblet granulate scores are stretched in comparison to the other granulate batches. This could be because the particles in the 0.5 gram riblet granulate batches have a wider particle size distribution or because there is something else about the particle characteristics in these batches that deviates from the other batches, e.g. the granulate could consist of small discs as mentioned earlier. This is also supported by the raw NIR spectra in Figure 35 and Figure 36 where there is much more baseline difference between spectra in the 0.5 g riblet batch granulate than in the 1.5 g riblet batch granulate. The 1.0 gram batches have a tendency that suggest that the same effect is present in this batch, however, with an average riblet thickness of 1.48 mm it is not that far off a ribbon production scale setting.

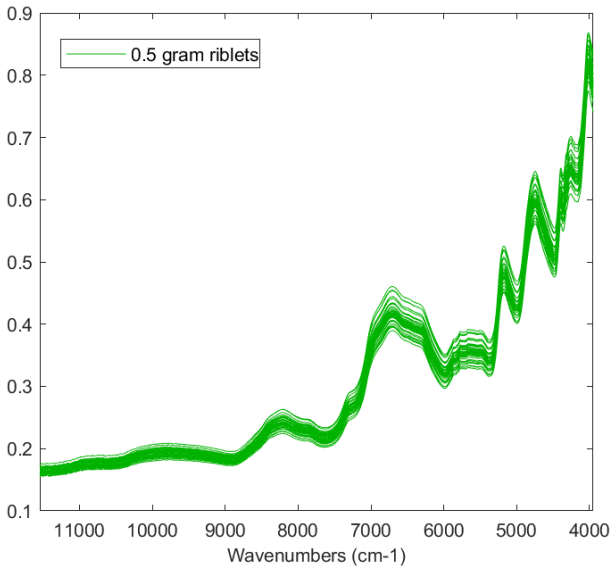

Figure 35: Raw NIR spectra of the 0.5 g riblet batch granulate made using the BSA formulation.

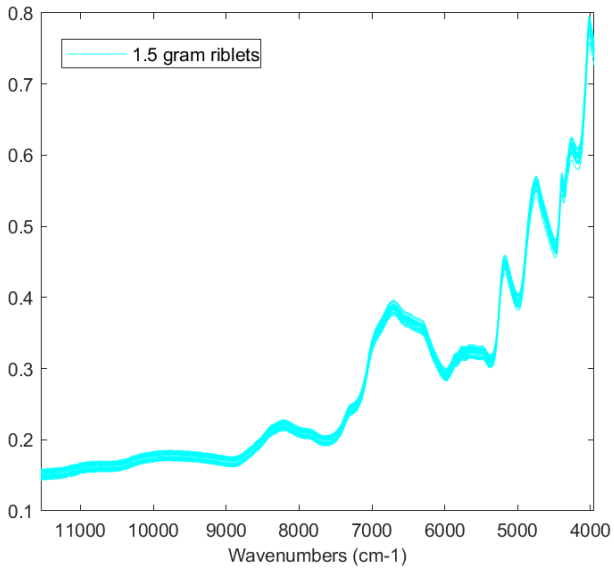

Figure 36: Raw NIR spectra of the 1.5 g riblet batch granulate made using the BSA formulation.

Each vial with granulate from the 1.0 g riblet batch granulate (BSA formulation) was remeasured with NIR three times each to assess the representativeness of each aliquot. Such an assessment is necessary as the new paper riffle splitter produces 12 aliquots instead of 8. The NIR measurements were predicted using the PCA model to find the scores on PC1 and PC2 (see Figure 37). Looking at the PCA scores plot in Figure 37 and comparing to the one in Figure 23, it is seen that the measurements are not as grouped by vial and the tendency that adjacent aliquots results in similar scores on PC1 and PC2 is not present here. There are fewer measurements of each vial, but it does not seem to be the case that changing the paper riffle splitter from a 8 pointed star to a 12 pointed star results in less representativeness.

It was decided to proceed with batches of 1.0 g, 1.5 g and 2.0 g riblets for production of granulate for the sample set.

Sample preparation

The aim is to be able to produce a sample set for calibration of an assay model on granulate that can predict BSA concentration and is robust towards particle and moisture variance. One BSA concentration level of 10.00 % has already been produced. Five more will be produced to span the concentration range 2.00 % to 15.00 %. The down-scaled process for production of granulate with different particle characteristics will be used to produce three levels of granulate. Desiccators will be used to moisturize the samples at four different relative humidities (RH). The overview can be seen in Table 3. A full factorial sample set with triplicates will be produced. This makes 216 samples in total.

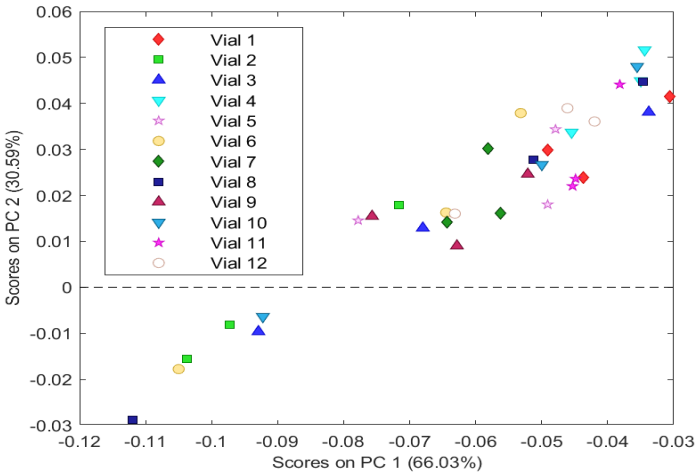

Figure 37: Prediction of PCA scores on PC1 and PC2 using the model from Figure 34 for 1.0 g riblet batch granulate (BSA formulation). Coloured according to vial number.

Table 3: Overview of controllable parameters and their levels used to produce the samples needed for calibration dataset and test set.

BSA concentration [%]	2.00	5.25	8.50	10.00	11.75	15.00
Particle variance caused by riblet quality [riblet in g]	1.0	1.5	2.0			
Moisture level [%RH]	11	33	43	62		

Three out of twelve aliquots from each granulate batch were chosen to form a triplicate set. The aliqouts chosen to form a triplicate set were evenly spaced around the paper riffle splitter to account for systematic error in the aliquotation according to Figure 38.

The samples were measured with NIR before and after moisturization with the MPA II equipment as described earlier. However, each measurement now used a resolution of 8 cm^{-1} and 64 scans in the range from 11550 cm^{-1} to 3950 cm^{-1}.

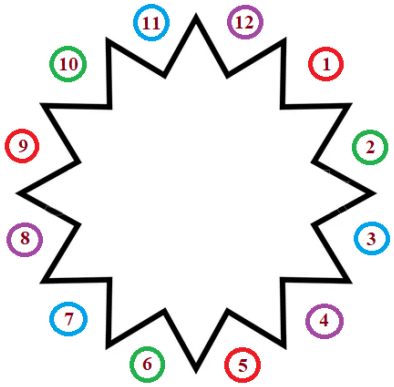

Figure 38: Example of chosen triplets of aliquots according to colour.

Moisturizing samples

The desiccators that were used to control the moisture content in the samples used RH levels of 11%, 33%, 43% and 62%. Two desiccators at each RH level was needed to store all the samples. This made 27 granulate samples in NIR vials per desiccator. The desiccators were prepared using the salts presented in Table 4 and water. The desiccators were placed on a magnetic stirrer overnight and hygrometers were used to measure %RH in the chambers. A difference in RH of around 2% was measured between the desiccator duplicates. However, this could also be due to hygrometer defects as a similar %RH difference was measured in the ambient atmosphere in the laboratory even though the hygrometers were positioned beside each other. The potential variance introduced by desiccator duplicates will be investigated later.

Table 4: Overview salts used to control %RH in desiccators.

%RH in desiccator	11	33	43	62
Salt used	LiCl	$MgCl_2 \cdot 6H_2O$	K_2CO_3	NH_4NO_3

To reduce potential systematic error as a result of difference between desiccator duplicates, the triplicates were distributed such that two NIR vials went into one desiccator and the third NIR vial went into the other. E.g. for the triplicate of reds in Figure 38, aliquot 1 and 9 would always go into the same desiccator and aliquot 5 would go into the other. This could render the possibility that a possible systematic error introduced by aliquotation would confound with the possible error introduced by desiccator duplicates. Therefore, vials 1 and 9 and vial 5 would alternate between going into desiccator A and desiccator B from batch to batch. E.g. for granulate batch 1, vial 1 and 9 would go into desiccator A and vial 5 would go into desiccator B. Then for granulate batch 2, vial 1 and 9 would go into desiccator B and vial 5 would go into desiccator A. The desiccators were sealed with vacuum grease after the vials were loaded. One vial with the most amount of granulate from one of the 62% RH desiccators was selected and measured before sealing. This vial would be measured with NIR every day in the morning and in the afternoon to track the moisturization. Choosing the vial containing the most amount of granulate from the desiccator where most moisture will be absorbed into the granulate was done based on the expectation that this vial would take the longest to reach equilibrium. A PCA model was calculated and updated twice a day using the NIR spectra of the selected vial. The spectra were pre-processed using SNV, 1st derivative and MC. PC1 for the PCA model describes 88 % of the total variance and from the PC1 loading in Figure 39 it is clear that this variance is because of the changing moisture content in the granulate as seen by the importance of the wavenumber range 5300 cm^{-1} to 4900 cm^{-1}. Within this range is where the first overtone of the $O-H$-stretch in H_2O can be found. Moisturization of the samples was stopped after 7 days as the change in scores on PC1 started to stagnate (see Figure 40). This stagnation indicated that moisture equilibrium between desiccator air and granulate was reached to a satisfactory degree. The vials were removed from the desiccators, sealed and measured using NIR.

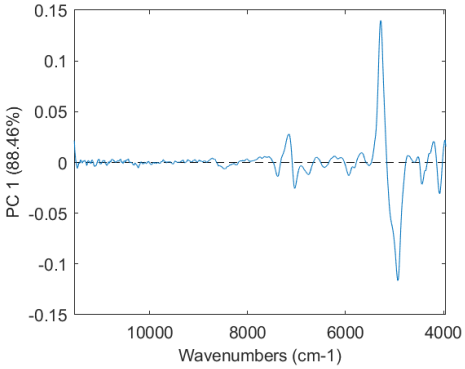

Figure 39: PC1 loading in the PCA model that was calculated using the vial measurements that were taken to track moisture development over time.

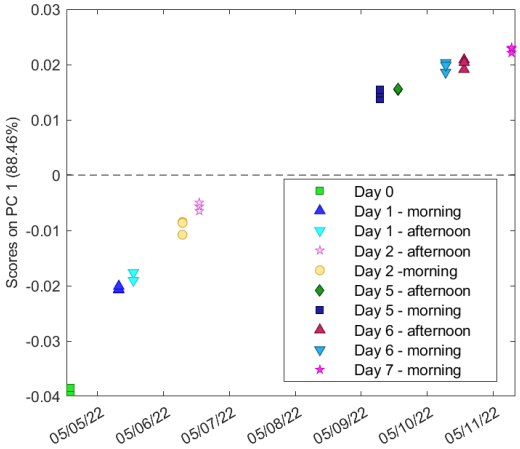

Figure 40: PCA scores on PC1 for vial used to track moisture development over time

PCA models were calibrated using sample measurements from and for each fraction of RH. The models were pre-processed using SNV and MC. Two of the four PCA models gave a loading that found variance due to water. If colouring the samples by desiccator (see Figure 41 and Figure 42), it is evident that there is difference between the desiccators. This was not intentional, however, it might not be an issue with this variance as the aim is to make a protein assay model that is robust towards water content in the granulate.

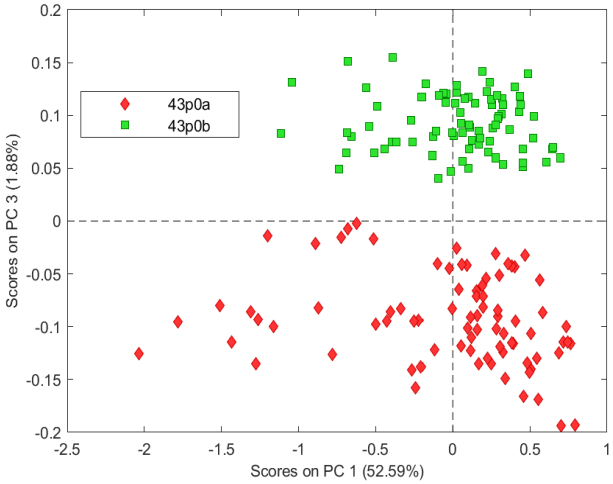

Figure 41: PCA scores plot using the fraction of samples that uses 43% RH. The scores are coloured according to desiccator.

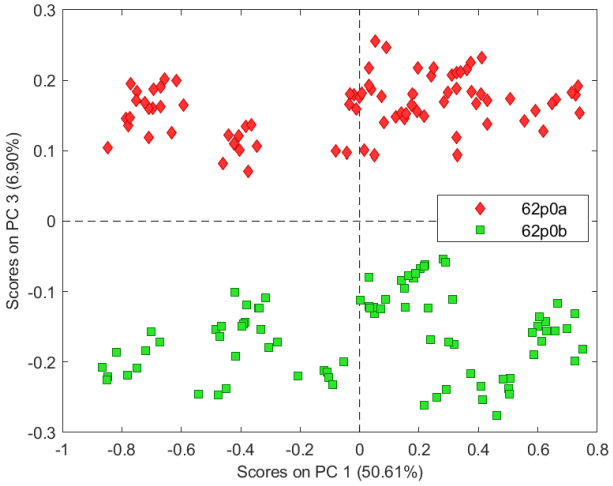

Figure 42: PCA scores plot using the fraction of samples that uses 62% RH. The scores are coloured according to desiccator.

The dataset

The sample set consisting of 216 samples was measured three times before and three times after moisturization. In total this produced 1296 measurements. Each measurement was given a unique filename consisting of the RH, the model API (BSA) concentration, the riblet weight, the vial number and the triplicate measurement (going from 0 to 2). E.g. for the sample using a RH of 11%, a BSA

concentration of 2%, a riblet weight of 1.0 g, with vial number 1 and first measurement, the measurement name would be RH11p0_API02p00_RW1p0_v1.0. This naming system was chosen to make it easy to import the meta data into MATLAB using a script. However, as more meta-data was found to be relevant for the dataset, an Excel spreadsheet was prepared containing riblet SF and desiccator number as well as the in-filename described meta-data. A MATLAB script was used to read off of the Excel spreadsheet to pull out files and meta-data by in-script defined parameters.

Robust calibration

Now that the dataset has been acquired, the robust calibration investigation part of this MSc project can be carried out. The investigation includes three subsections. Subsection one will be a continued investigation into the variance in the dataset. Subsection two will test different regression, pre-processing and variables selection techniques to try and optimize regression models. Subsection three will try an mimic different un-expected changes in the sample matrix and test what regression models that are most robust.

Subsection one

The raw NIR spectra are presented in Figure 43 and Figure 44. The red group is generally dominant for the spectra taking higher absorbance. The red group indicates the group of granules made of riblets with a weight of 1.0 g. There is also more scattering in the red group. This is especially visible in Figure 44 that contains the measurements taken after moisturization. If taking the standard deviation of the spectra's absorbance at each wavenumber, it can be seen how the two datasets differs in scattering (see Figure 45). The largest difference in scattering is in the spectrum range where water gives a signal. The moisture also seems to interact with the particle characteristics as there seem to be more scattering in the spectra after moisturization at all wavenumbers below 8500 cm^{-1}.

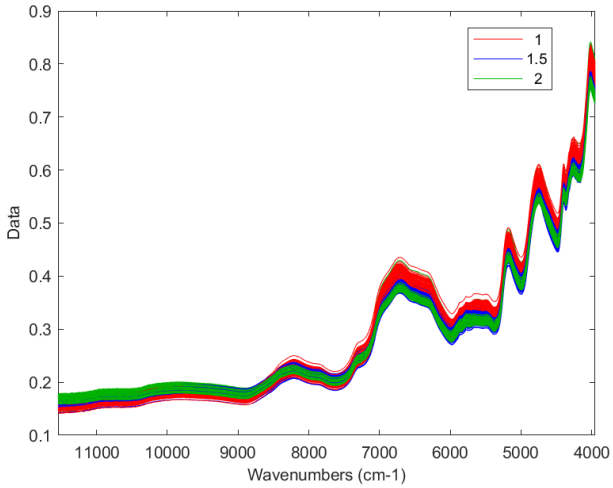

Figure 43: Raw NIR spectra of samples before moisturization. Coloured according to riblet weight.

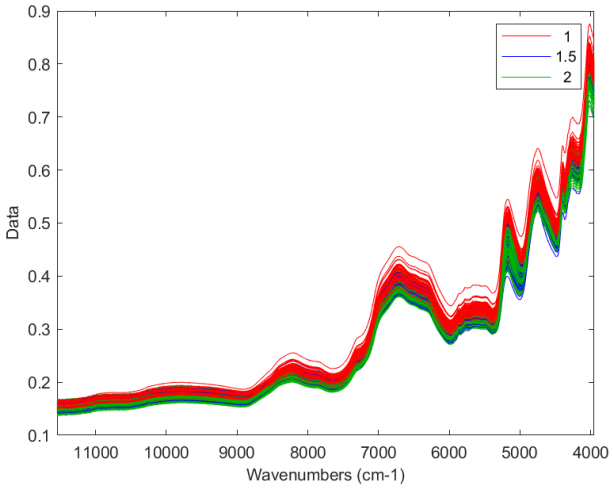

Figure 44: Raw NIR spectra of samples after moisturization. Coloured according to riblet weight.

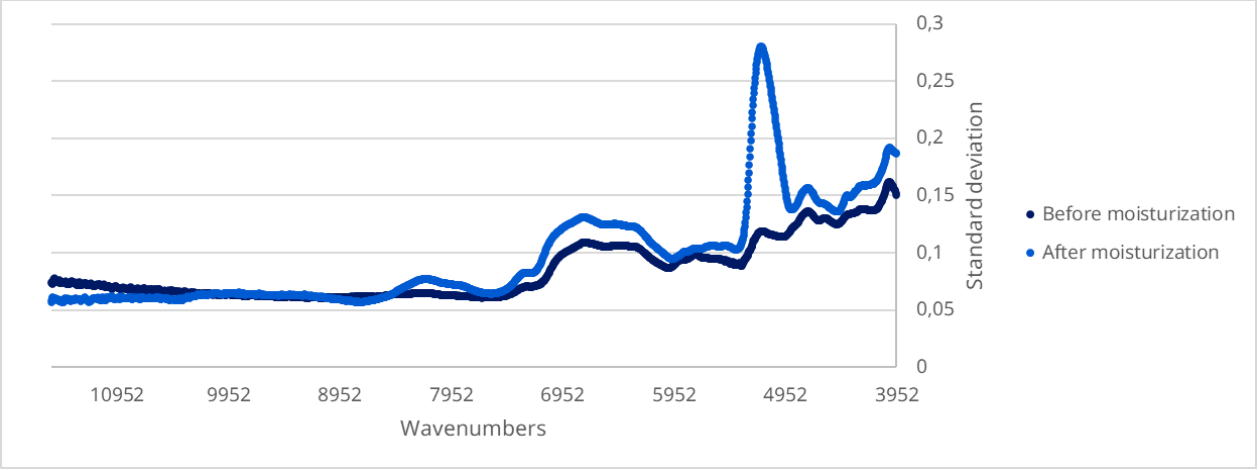

Figure 45: Standard deviation taken at each wavenumber for the two datasets that includes measurements of the samples before and after moisturization, respectively.

A PCA model was calibrated using measurements after moisturization. The spectra were first pre-processed using SNV and MC. When measuring through the bottom of the vial, only a fraction of the entire granulate sample in the vial gets measured. The vial was measured three times and it was turned and rotated between each measurement. The measurement representativeness of the sample can be increased if taking the average spectrum of the triplicate measurements of each vial. The effect of this can be seen if inspecting the Hotelling T^2 vs Q Residuals plots in Figure 46 and Figure 47. It turns out that vial 6 from the 8.5% BSA concentration and 1.0 g riblet granulate batch that was moisturized under 43% RH is an outlier in the calibrated PCA model. PCA scores plots are inspected to see if the PCA model catches variance in the data that can be assigned to the different controllable parameters that are listed in Table 3. PC1 and PC2 catches the variance caused by water content and BSA concentration, respectively (see Figure 48 and Figure 49). The loadings plot for PC2 can be seen in Figure 51 and compared with the NIR absorbance spectra of the three raw ingredients in Figure 50. It is difficult to correlate the PC2 loading to the BSA spectrum. But if the MCC spectrum is subtracted from the BSA spectrum, then the same pattern as the PC2 loading appears (see Figure 52). This makes sense as the higher the concentration of BSA, the smaller the concentration of MCC. PC3 seems to catch variance related to particle size but this is not as evident as it was for PC1 and PC2 for the two other controlled parameters (see Figure 53). As was also noticed earlier, the addition of variance in water content seems to interfere with the variance related to particle size. This time it is suggested by the much better description of variance related to particle size by PC1 from a twin PCA model that was calibrated using the dataset with measurements of the granulate samples before moisturization (see Figure 54). The dataset with measurements of the granulate samples before moisturization contain much less variance in water content. In Figure 55, the before and after moisturization datasets have both been used to calibrate a single PCA model. Here the “Ambient” group corresponds to before moisturization. It scores in-between the group that went into the 11% RH desiccators and the group that want into the 33% RH desiccators. The laboratory in which the most of the dry granulation

process took place was temperature and humidity controlled. The ambient RH in the laboratory was around 25% which fits with what is observed in the data.

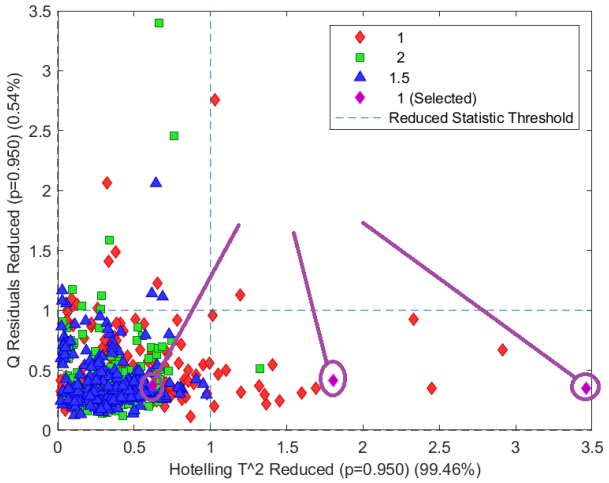

Figure 46: Hotelling T^2 (Reduced) vs Q Residuals (Reduced) plot from PCA model using all measurements from after moisturization. The points have been coloured according to tablet weight and one of the measurements that scores high on Hotellings T^2 has been selected and encircled along with its' two other triplicate measurements.

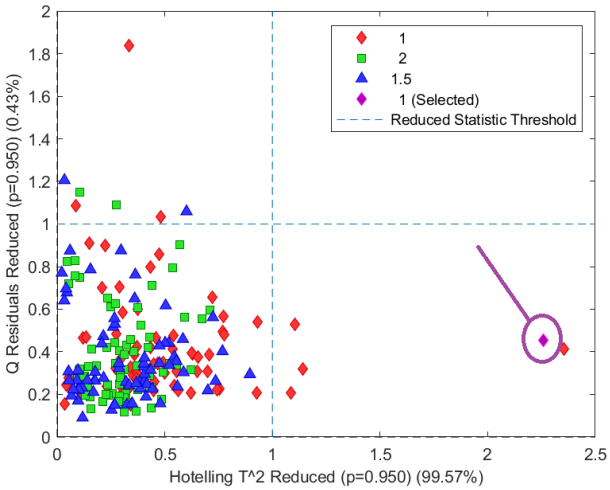

Figure 47: Hotelling T^2 (Reduced) vs Q Residuals (Reduced) plot from PCA model using means of triplicate measurements from after moisturization. The selected and encircled point represent the mean of the triplicate set selected in Figure 46.

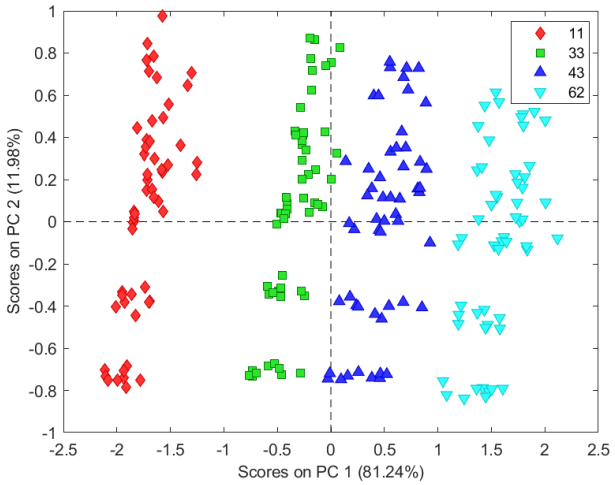

Figure 48: PCA scores plot. PCA model used the sample measurements after moisturization and pre-processing with SNV and MC. Coloured according to %RH.

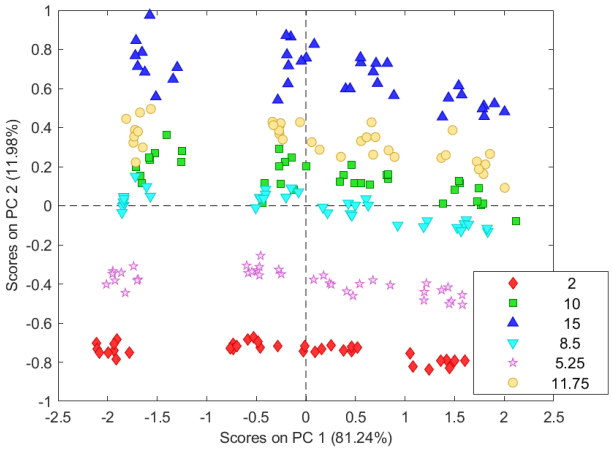

Figure 49: PCA scores plot. PCA model used the sample measurements after moisturization and pre-processing with SNV and MC. Coloured according to BSA concentration.

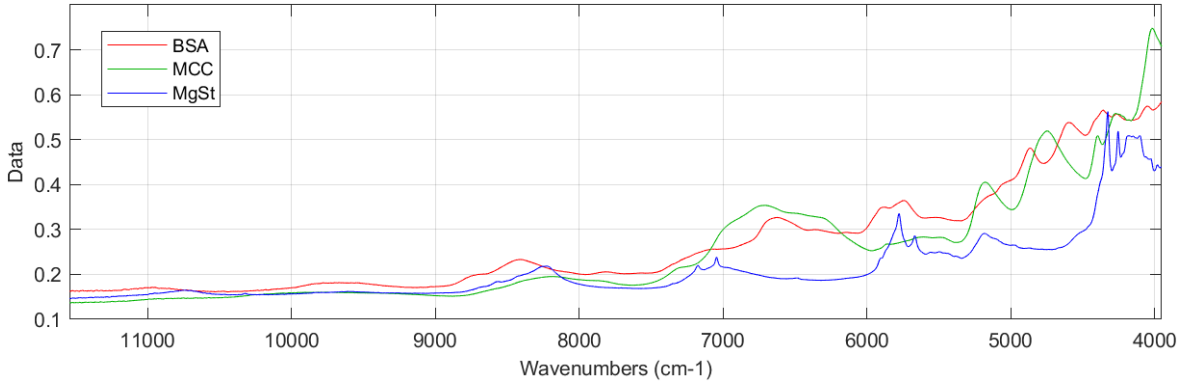

Figure 50: NIR absorbance spectra of the three raw ingredients.

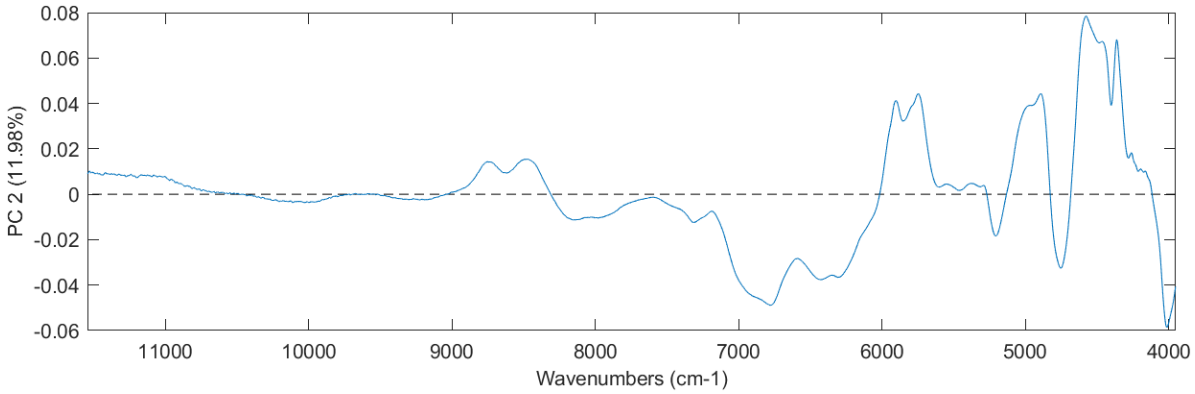

Figure 51: PC2 loading plot from the PCA model calibrated on the sample measurements after moisturization and pre-processing with SNV and MC.

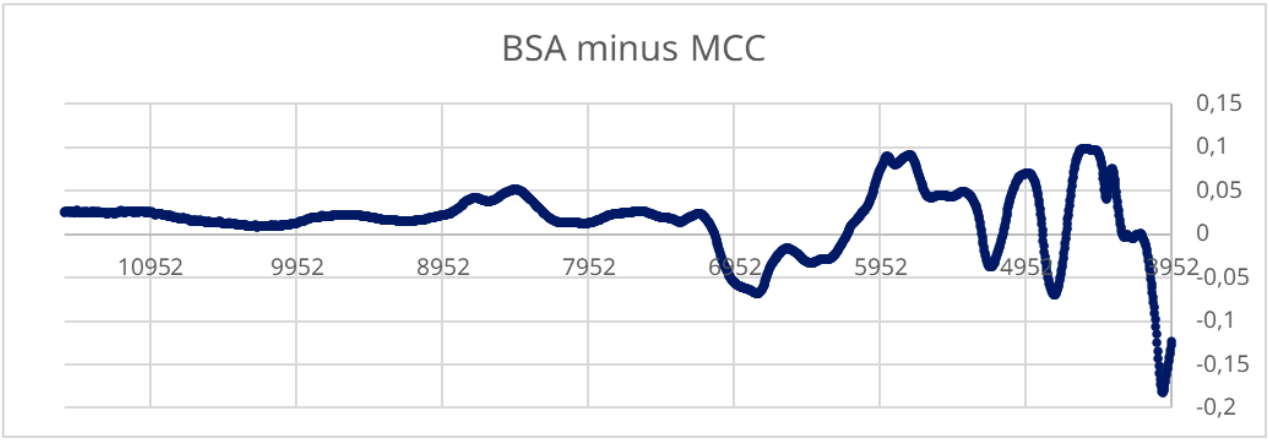

Figure 52: The resulting spectrum after subtracting the MCC spectrum from the BSA spectrum in Figure 50.

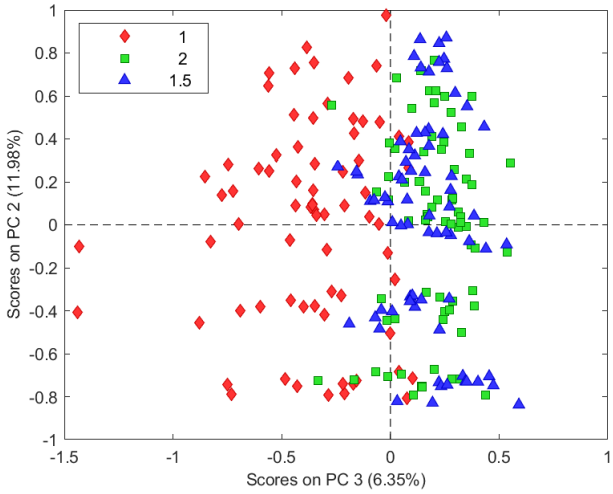

Figure 53: PCA scores plot. PCA model used the sample measurements after moisturization and pre-processing with SNV and Mean Centring. Coloured according to riblet weight in grams.

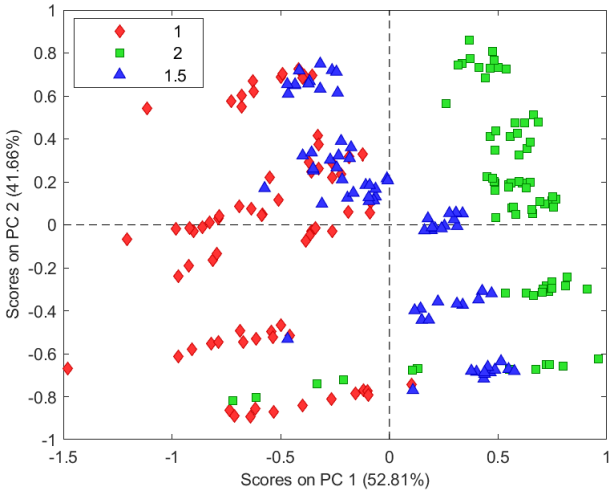

Figure 54: PCA scores plot. PCA model used the sample measurements before moisturization and pre-processing with SNV and Mean Centring. Coloured according to riblet weight in grams.

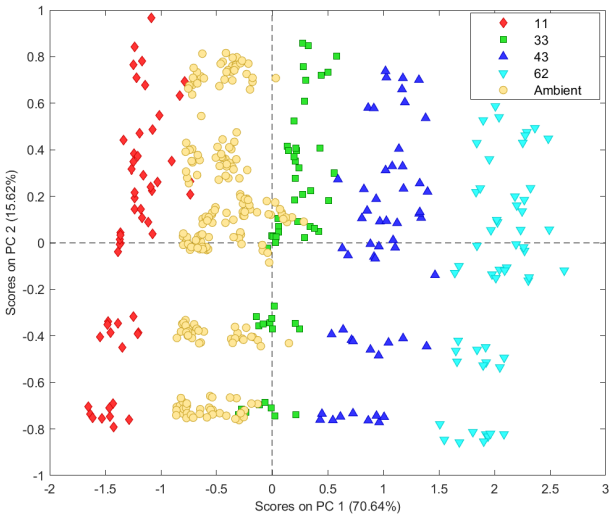

Figure 55: PCA scores plot that uses both the before and after moisturization sample measurements as dataset.

Subsection two

Firstly, different pre-processing methods and variables selections were tried out to optimize a PLS regression model for prediction of BSA concentration. All models used mean NIR absorbance spectrum measurements from the different triplicate sets where two of the three vials were used for calibration. E.g. from Figure 38 the red group using vial 1, 5 and 9 is a triplicate set. As explained earlier vial 1 and 9 went into one desiccator and vial 5 went into the other. Therefore, measurements

of vial 1 and 5 were used for optimization of a regression model and the measurement of vial 9 was used for test set. This meant that the calibration block would use 144 samples and the test set would use 72 samples. All models used venetian blinds as cross-validation with blind size of 2 and 11 splits such that each set of duplicate samples formed its' own blind.

Secondly, a few of the best performing models were selected and validated using the test set. The models that perform well and/or differs from the others were chosen for Subsection three.

Optimizing the PLS regression model

Several different pre-processing methods were selected: Mean Centring, Autoscaling, SNV, MSC, EMSC, 1st derivative, 2nd derivative and combinations of those. The whole spectrum range was used at first. Then variables selection strategies were tried out. The primary focus was on optimizing a PLS regression model. The following is a presentation of:

1. Selected models using assessment metrics such as RMSEC, -RMSECV, number of latent variables (LVs) and R^2 values.
2. Observations that were made during the investigation.

The first eight models that were calibrated using the whole spectrum range are presented in Table 5. All models were optimized on number of LVs and detection for outliers using Q Residuals and Hotelling T^2 values. Judging from the metrics, model 5 that uses 1st derivative produces the better model.

Table 5: Overview of different calibrated PLS regression models with assessment metrics. RMSE-values are coloured according to size of value where green is lowest and red is highest.

Model #	LVs	X pre-processing	X Include size	RMSEC	RMSECV	RMSE Ratio	R^2 (Cal)	R^2 (CV)
Model 1	4	Mean Center	143 x 1899	0,5048	0,5279	1.046	0.9859	0.9846
Model 2	4	SNV , Mean Center	143 x 1899	0,5111	0,5357	1.048	0.9855	0.9841
Model 3	4	MSC (Mean) , Mean Center	143 x 1899	0,5107	0,5359	1.049	0.9855	0.9841
Model 4	4	EMSC (Extended Scatter Correction) , Mean Center	143 x 1899	0,5104	0,5353	1.049	0.9856	0.9841
Model 5	4	1st Derivative (order: 2, window: 15 pt, tails: weighted) , Mean Center	143 x 1899	0,3889	0,4308	1.108	0.9916	0.9897
Model 6	3	2nd Derivative (order: 2, window: 15 pt, tails: weighted) , Mean Center	143 x 1899	0,4888	0,5413	1.107	0.9868	0.9838
Model 7	3	SNV , 1st Derivative (order: 2, window: 15 pt, tails: weighted) , Mean Center	143 x 1899	0,5119	0,5336	1.042	0.9855	0.9842
Model 8	3	1st Derivative (order: 2, window: 15 pt, tails: weighted) , SNV , Mean Center	143 x 1899	0,5129	0,5469	1.066	0.9854	0.9834

The calibration plot for model 5 can be seen in Figure 56. The PLS scores plot from model 5 in Table 5 can be seen in Figure 56 and Figure 57. The scores plots are coloured by BSA concentration and desiccator, respectively. Using 1st derivative as pre-processing makes the PLS regression model really capable at quantifying the variance that is caused by water content. It can even separate the samples that went into different desiccators. When looking at Figure 56, there is some overlapping of the scores from different BSA concentrations. When comparing the loading for LV1

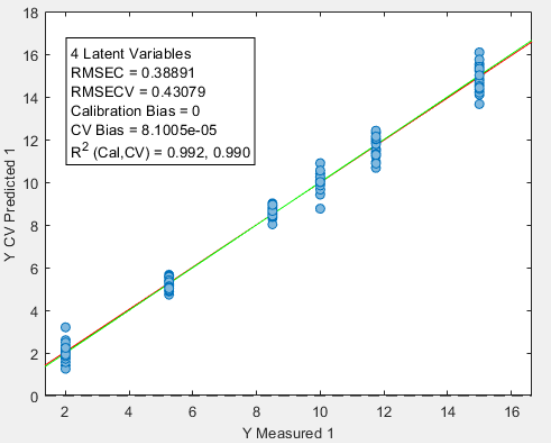

Figure 56: Calibration plot for model 5 in Table 5

with the 1st derivative of the loading for PC2 in Figure 51, it is seen that they find the same variance in the two datasets (see Figure 60).

The PLS scores plot from model 2 in Table 5 can be seen in Figure 58 and Figure 59. The scores plots are coloured by BSA concentration and relative humidity, respectively. Both LV1 and LV2 catch variance that is caused by both water content and BSA concentration. The loadings in Figure 61 confirms that LV1 and LV2 both, but oppositely, catch variance related to water content. So, model 5 was better at isolating the variance caused by water content, however, there is better defined groupings related to BSA concentration here when using LV1 and LV2 than what was seen for model 5. It seems that for both model 2 and model 5 in Table 5, the water content accounts for much of the total variance in the data even after pre-processing. Some variables selection might be beneficial.

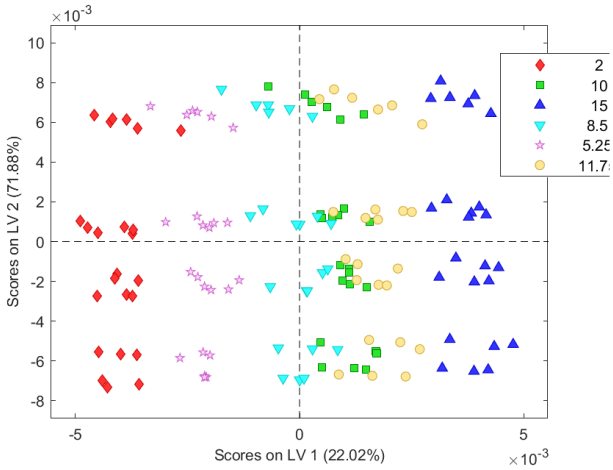

Figure 57: PLS scores plot for model 5 in Table 5. It is coloured according to BSA concentration.

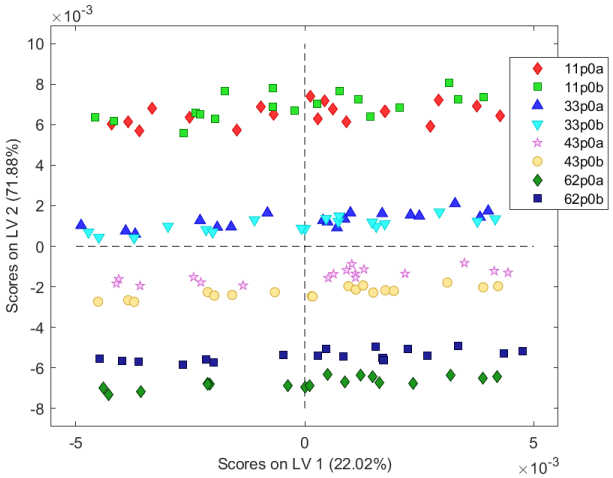

Figure 58: PLS scores plot for model 5 in Table 5. It is coloured according to desiccator.

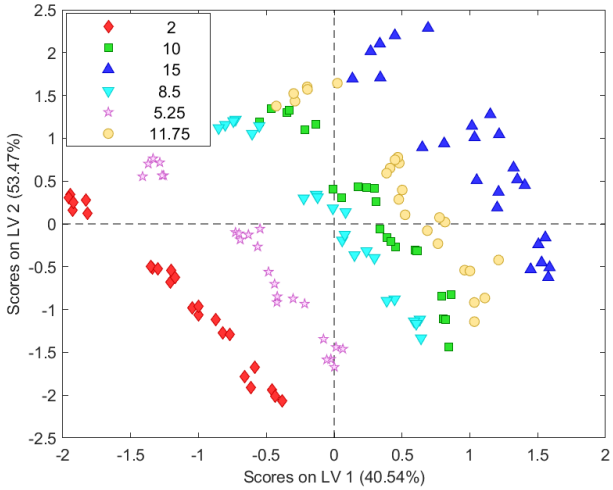

Figure 59: PLS scores plot for model 2 in Table 5. It is coloured according to BSA concentration.

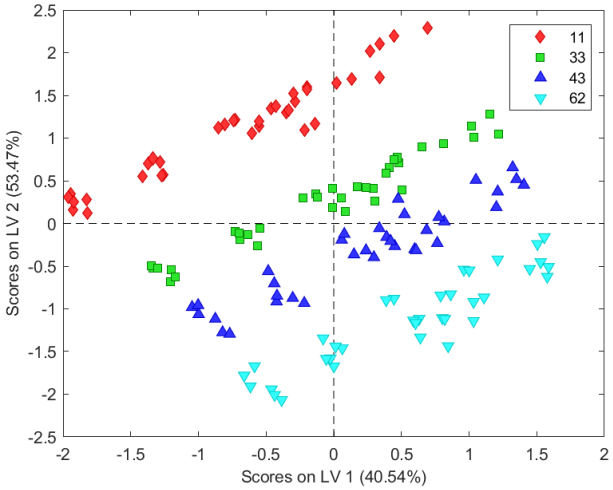

Figure 60: PLS scores plot for model 2 in Table 5. It is coloured according to %RH.

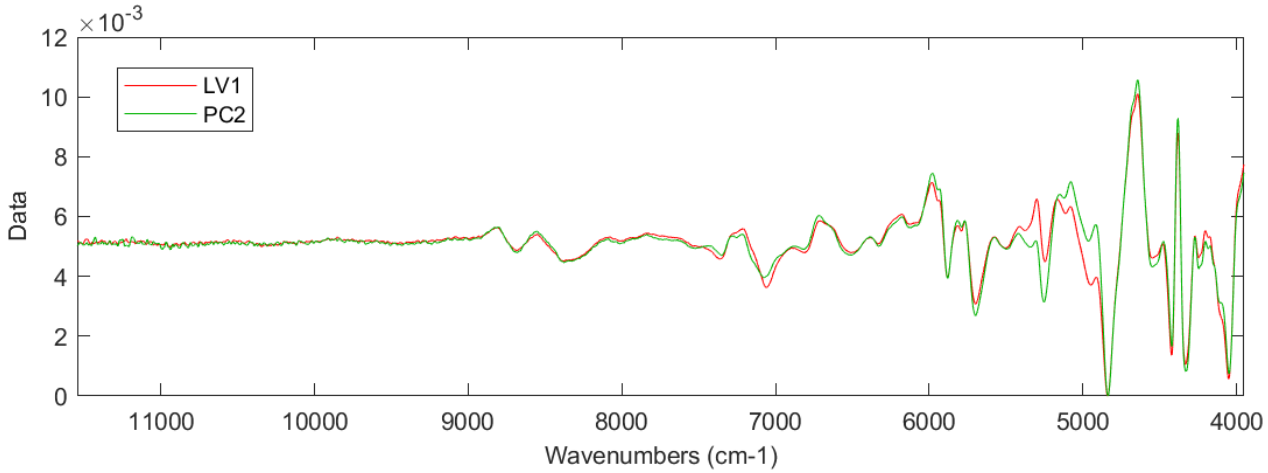

Figure 61: Loadings plot using LV1 from PLS model 5 in Table 5 and PC2 from the PCA model from Subsection one). PC2 has been pre-processed with 1st derivative.

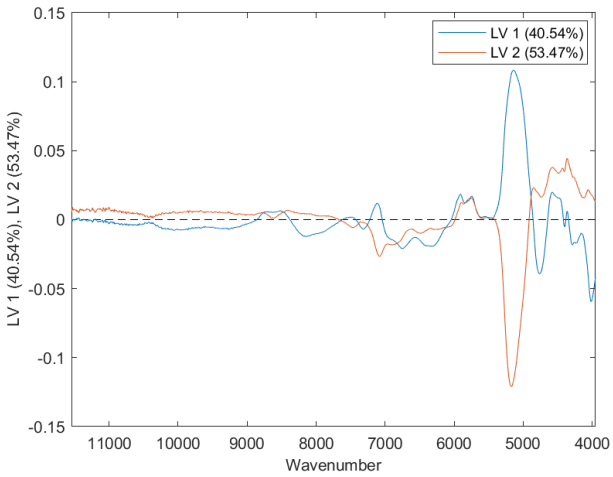

Figure 62: PLS loadings plot for model 2 in Table 5 including loadings for LV1 and LV2.

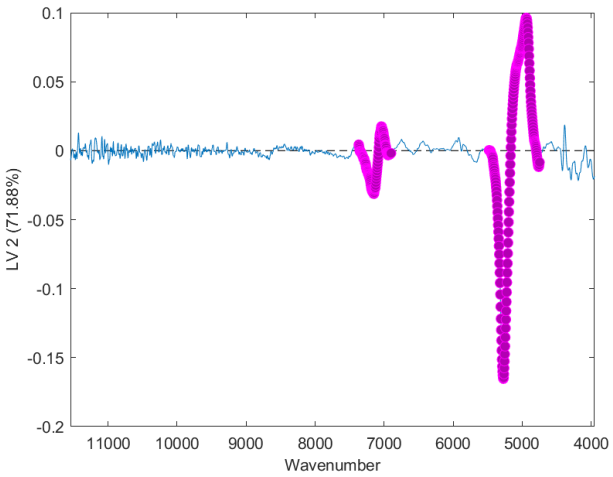

Figure 63: Model 5 in Table 5 PLS loading LV2 plot including selection of regions important for describing water content.

Variables selection

Different variables selection strategies will be used for the models presented in Table 5. As just discussed, most of the variance seen in the models are related to water content. So, the first strategy will be to identify the wavenumbers that explain water content and exclude these from the dataset. The second strategy will utilize an automatic variables selection method.

The loading plot for LV2 in model 5 (see Figure 62) is used to identify the wavenumbers that describe water content. The selected wavenumbers correspond to the 1st and 2nd overtone of the $O-H$-stretch

in water. All the models in Table 5 were recalculated excluding the wavenumbers that describe water content. The new models are presented in Table 6.

Table 6: Overview of different calibrated PLS regression models with assessment metrics. The wavenumbers that describe water content have been excluded. RMSE-values are coloured according to size of value where green is lowest and red is highest.

Model #	LVs	X pre-processing	X Include size	RMSEC	RMSECV	RMSE Ratio	R^2 (Cal)	R^2 (CV)
Model 9	4	Mean Center	143 x 1593	0,58	0,6113	1.054	0.9814	0.9793
Model 10	4	SNV , Mean Center	143 x 1593	0,4282	0,4782	1.117	0.9898	0.9873
Model 11	4	MSC (Mean) , Mean Center	143 x 1593	0,4283	0,4782	1.117	0.9898	0.9873
Model 12	4	EMSC (Extended Scatter Correction) , Mean Center	143 x 1593	0,4785	0,5045	1.054	0.9873	0.9859
Model 13	4	1st Derivative (order: 2, window: 15 pt, tails: weighted) , Mean Center	143 x 1593	0,4037	0,4445	1.101	0.991	0.989
Model 14	3	2nd Derivative (order: 2, window: 15 pt, tails: weighted) , Mean Center	143 x 1593	0,4668	0,5536	1.186	0.9879	0.983
Model 15	3	SNV , 1st Derivative (order: 2, window: 15 pt, tails: weighted) , Mean Center	143 x 1593	0,5026	0,521	1.037	0.986	0.985
Model 16	3	1st Derivative (order: 2, window: 15 pt, tails: weighted) , SNV , Mean Center	143 x 1593	0,5035	0,548	1.088	0.9859	0.9834

The models using pre-processing techniques SNV, MSC and EMSC have improved their performance. But it is still the model that uses 1st derivative that performs the best. However, this model did not benefit from this variables selection.

The models using:

- SNV and Mean Centring
- 1st derivative and Mean Centring
- SNV, 1st derivative and Mean Centring

were selected for further optimization through automatic variables selection. The automatic variables selection method that was used was forward IPLS using automatic selection of number of intervals and with an interval size of 50. The results are presented in Figure 63, Figure 64, Figure 65 and Table 7. All three models uses the wavenumber range from 6500 cm^{-1} to 6000 cm^{-1}. This is a range where BSA has higher absorbance in the NIR spectrum than MCC and MgSt (see Figure 50). Only the model using SNV, 1st derivative and MC would produce a better model after the IPLS variables selection when using the same number of LVs.

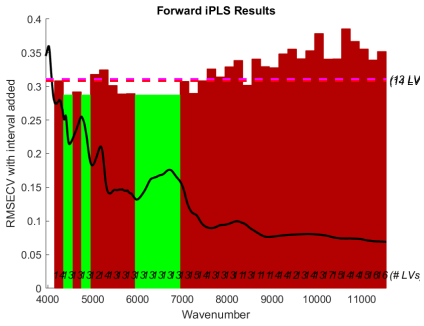

Figure 64: Variables selection results using forward IPLS. The pre-processing was SNV and Mean Centring.

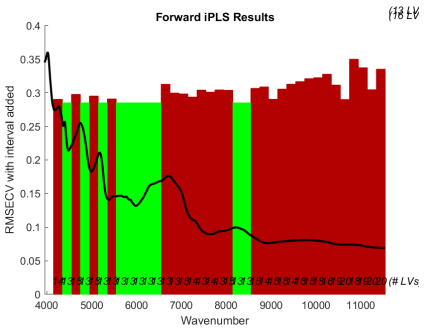

Figure 65: Variables selection results using forward IPLS. The pre-processing was 1st derivative and Mean Centring.

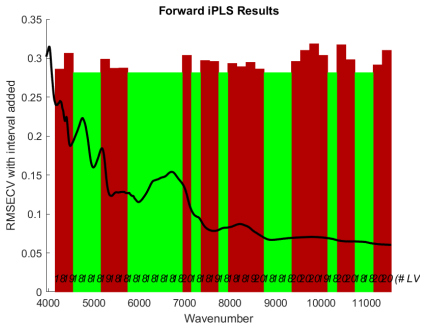

Figure 66: Variables selection results using forward IPLS. The pre-processing was SNV, 1st derivative and Mean Centring.

Table 7: Overview of different calibrated PLS regression models with assessment metrics. Forward IPLS variables selection method has been used. RMSE-values are coloured according to size of value where green is lowest and red is highest.

Model #	LVs	X pre-processing	X Include size	RMSEC	RMSECV	RMSE Ratio	R^2 (Cal)	R^2 (CV)
Model 17	9	SNV , Mean Center	143 x 350	0,2983	0,3545	1.189	0.9951	0.993
Model 18	5	1st Derivative (order: 2, window: 15 pt, tails: weighted) , Mean Center	143 x 500	0,3773	0,4049	1.073	0.9921	0.9909
Model 19	4	SNV , 1st Derivative (order: 2, window: 15 pt, tails: weighted) , Mean Center	143 x 850	0,4774	0,5266	1.103	0.9874	0.9846

Conclusion on PLS regression model optimization

After this optimization of PLS regression models, four models are chosen for further assessment. The four models are presented in Table 8. Model 1 was chosen as a base-model. It only uses MC as pre-processing and the entire spectrum. Model 5 was judged to be the best model calibration when taking the RMSE-values and the number of LVs into account. Model 10 was chosen as an alternative to model 5. If either model 5 or model 10 gives a poor robustness, it would be interesting to see how the other performs. Model 19 was chosen as it uses a mix of the pre-processing from model 5 and model 10 and because it performs decently.

Table 8: Overview of the selected calibrated PLS regression models with assessment metrics. They are to be used for further assessment.

Model #	LVs	X pre-processing	X Include size	RMSEC	RMSECV	RMSE Ratio	R^2 (Cal)	R^2 (CV)
Model 1	4	Mean Center	143 x 1899	0,5048	0,5279	1.046	0.9859	0.9846
Model 5	4	1st Derivative (order: 2, window: 15 pt, tails: weighted) , Mean Center	143 x 1899	0,3889	0,4308	1.108	0.9916	0.9897
Model 10	4	SNV , Mean Center	143 x 1593	0,4282	0,4782	1.117	0.9898	0.9873
Model 19	4	SNV , 1st Derivative (order: 2, window: 15 pt, tails: weighted) , Mean Center	143 x 850	0,4774	0,5266	1.103	0.9874	0.9846

Optimizing the SVM regression model

As an alternative to PLS regression modelling, SVM regression modelling was tried. This is a regression technique that is also being used at Novo Nordisk. The three pre-processing combinations used for model 5, model 10 and model 19 were tried as well as with and without the wavenumber regions that describe water content. Also, Autoscaling was used instead of MC for some of the models. The calibrated models are presented in Table 9. A noticeable difference between the previously calibrated PLS regression models and some of the SVM regression models is that the RMSE ratio values are larger for the SVM regression models. This could indicate that those models are less robust towards changes in the sample matrix or that overfitting occurs. Of the nine models presented in Table 9, two are chosen for further assessment: Model 24 was chosen as it has decent RMSEC and -CV values and a relatively low RMSE ratio. Model 26 was chosen as it has a relatively low RMSECV and a fair RMSE ratio. Also, model 26 uses Autoscaling which deviates from the other models that were selected. The calibration plot for model 26 can be seen in Figure 67.

Table 9: Overview of calibrated SVM regression models with assessment metrics. The RMSE-values have been coloured according to size of value where green/white is lowest and red/dark grey is highest.

Model #	X pre-processing	X Include size	RMSEC	RMSECV	RMSE Ratio	R^2 (Cal)	R^2 (CV)
Model 20	SNV , Mean Center	143 x 1899	0,2675	0,4221	1.578	0.9961	0.9902
Model 21	SNV , Mean Center	143 x 1593	0,1984	0,3791	1.911	0.9978	0.9921
Model 22	1st Derivative (order: 2, window: 15 pt, tails: weighted) , Mean Center	143 x 1899	0,7395	0,8283	1.120	0.9788	0.9743
Model 23	1st Derivative (order: 2, window: 15 pt, tails: weighted) , Mean Center	143 x 1593	1,0240	1,1530	1.126	0.9705	0.9661
Model 24	SNV , 1st Derivative (order: 2, window: 15 pt, tails: weighted) , Mean Center	143 x 1899	0,4275	0,4894	1.145	0.9901	0.987
Model 25	SNV , 1st Derivative (order: 2, window: 15 pt, tails: weighted) , Mean Center	143 x 1593	0,4282	0,4965	1.159	0.9902	0.9867
Model 26	SNV , Autoscale	143 x 1593	0,2945	0,3887	1.320	0.9952	0.9917
Model 27	1st Derivative (order: 2, window: 15 pt, tails: weighted) , Autoscale	143 x 1593	0,2184	0,4334	1.984	0.9976	0.9901
Model 28	SNV , 1st Derivative (order: 2, window: 15 pt, tails: weighted) , Autoscale	143 x 1593	0,2904	0,4676	1.610	0.9956	0.9883

Validation of the selected models

Six regression models (four PLS and two SVM) has been selected for further assessment. The test set will be tested on the models as validation.

Model 24 produced and RMSEP value of 1.5953. This is too far off from the RMSEC and -CV values, therefore, this was removed from further investigations. The final five models that will be tested for their robustness towards changes in the sample matrix in Subsection three are summarized in Table 10

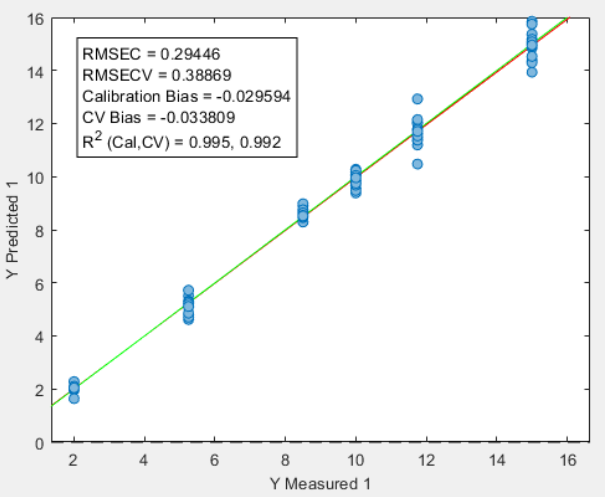

Figure 67: Calibration plot for model 26 in Table 9.

Table 10: Overview of the final selection of calibrated regression models with assessment metrics.

Model #	Regression type	LVs	X pre-processing	X Include size	RMSEC	RMSECV	RMSEP	RMSE Ratio	R^2 (Cal)	R^2 (CV)
Model 1	PLS	4	Mean Center	143 x 1899	0,5048	0,5279	0,5324	1.046	0.9859	0.9846
Model 5	PLS	4	1st Derivative (order: 2, window: 15 pt, tails: weighted) , Mean Center	143 x 1899	0,3889	0,4308	0,4805	1.108	0.9916	0.9897
Model 10	PLS	4	SNV , Mean Center	143 x 1593	0,4282	0,4782	0,4776	1.117	0.9898	0.9873
Model 19	PLS	4	SNV , 1st Derivative (order: 2, window: 15 pt, tails: weighted) , Mean Center	143 x 850	0,4774	0,5266	0,5105	1.103	0.9874	0.9846
Model 26	SVM	-	SNV , Autoscale	143 x 1593	0,2945	0,3887	0,3695	1.320	0.9952	0.9917

Subsection three

This subsection will test the robustness of the five selected regression models. It will include four simulated scenarios that mimics different unexpected changes in the sample matrix:

- Simulation 1: The dataset will include all sample measurements from the three lowest RH levels (11%, 33% and 43%) and will use the sample measurements from the highest RH level (62%) as test set. This simulation will test what regression model and pre-processing method that is most robust to the situation where the test samples have gained moisture above the calibration samples.
- Simulation 2: The dataset will include all samples measurements from the three highest RH levels (33%, 43% and 62%) and will use the sample measurements from the lowest RH level (11%) as test set. This simulation will test what regression model and pre-processing method that is most robust to the situation where the test samples are more dry than the calibration samples i.e. samples have dried out.
- Simulation 3: The dataset will include all sample measurements from the granulates that were made of the more massive riblets (1.5 g and 2.0 g) as these gave granulate with relatively smaller particles. The test set will use sample measurements of the granulate that was made with the lightest riblet (1.0 g). The project aims to test robustness towards larger than normal particles.
- Simulation 4: The dataset will include all sample measurements from the granulate that were made of the lighter riblets (1.0 g and 1.5 g) as these gave granulate with relatively larger particles. The test set will use sample measurements of the granulate that was made with the most massive riblet (2.0 g). The project aims to test robustness towards smaller than normal particles.

The five models were tested in each of the four simulated scenarios. The resulting RMSEP values are presented in Table 11. The models generally perform better when the unexpected changes to the sample matrix are because of changes to the particle size of the granulate. The best overall performing model is the PLS regression model that uses 1st derivative and MC as pre-processing. It especially performs well in simulation 3 and 4. This makes sense as taking the 1st derivative gets rid of the offsets that are caused by different particle sizes. In simulation 1, it is the SVM regression model that uses SNV and Autoscale as pre-processing that performs the best.

Table 11: The resulting RMSEP values after robustness testing for each model in each of the four simulated scenarios. Coloured according to value size.

		Simulation 1	Simulation 2	Simulation 3	Simulation 4
Regression type	X pre-processing	RMSEP	RMSEP	RMSEP	RMSEP
PLS	Mean Center	0,8764	1,0030	0,6201	0,5816
PLS	1st Derivative (order: 2, window: 15 pt, tails: weighted) , Mean Center	0,6064	0,5263	0,4487	0,5261
PLS	SNV , Mean Center	0,79	0,9793	0,5074	0,6915
PLS	SNV , 1st Derivative (order: 2, window: 15 pt, tails: weighted) , Mean Center	0,7062	1,1040	0,6054	0,6372
SVM	SNV , Autoscale	0,492	0,7740	0,5856	0,5212

Performance

One thing is robustness, another is the performance. To evaluate if the performance is good enough, the metric called the "precision-tolerance"-ratio (p/t-ratio) is used.

P in the P/T-ratio is the precision of the NIR method when analysing a product that is produced on target. T is the specification interval. If the specifications requires that the product should operate within +/-15% of 100% then the specification interval goes from 85% to 115% and T=30%.

A good performance results in a P/T-ratio of <10%. If the P/T-ratio is between 10% and 30% then the performance is acceptable. If the P/T-ratio is >30% then the method is unfit for its purpose.

The five models in Table 11 can be evaluated on their P/T-ratio. It is assumed that they will be used to measure a product with 9% BSA concentration. +/-15% of 9% is 7.65% and 10.35% this give a $T = 10.35\% - 7.65\% = 2.7\%$. Their P-values will be set to their RMSEP-values and thus the PT-ratios can be calculated (see Table 12).

Table 12: The resulting P/T-values for each model in each of the four simulated scenarios. Coloured according to value size.

		Simulation 1	Simulation 2	Simulation 3	Simulation 4
Regression type	X pre-processing	P/T-ratio	P/T-ratio	P/T-ratio	P/T-ratio
PLS	Mean Center	0,3245926	0,3714815	0,2296667	0,2154074
PLS	1st Derivative (order: 2, window: 15 pt, tails: weighted) , Mean Center	0,2245926	0,1949259	0,1661852	0,1948519
PLS	SNV , Mean Center	0,2925926	0,3627037	0,1879259	0,2561111
PLS	SNV , 1st Derivative (order: 2, window: 15 pt, tails: weighted) , Mean Center	0,2615556	0,4088889	0,2242222	0,236
SVM	SNV , Autoscale	0,1822222	0,2866667	0,2168889	0,193037

After inspection of the P/T-ratios in Table 12, it can be concluded that none of the models has a good performance. Most of the models has acceptable performance in the different scenarios. But the performance was unacceptable in four of the simulation tests divided between the PLS models that used 1) MC, 2) SNV and MC and 3) SNV, 1st derivative and MC as pre-processing. Only the PLS

model that used 1st derivative and MC and the SVM model that used SNV and Autoscaling gave acceptable performance throughout the simulation tests.

Conclusion

This project consisted of two parts. The first part attempted to develop a down-scaled granulation process for production of granulate. Two granulate attributes had to be controllable in the down-scaled granulation process: The granulate particle size and the model API concentration. The project used a QbD approach to develop a process for production of granulate where the particle size was controllable. The QbD approach included on-going investigations and evaluation using NIR spectroscopy. Firstly, the compaction step was investigated. Here knowledge was formed about riblet SF dependence on pressure used during compaction. It was found that SF variance could occur within a single riblet and that it was important to fill the piston die carefully before compaction of the riblets. Secondly, the granulation step was investigated. Here knowledge about the riblet quality's impact on granulate quality was created. The investigation found that the particle size in the granulate could be controlled through the amount of powder mass used during compaction of the riblets. Riblet specifications were defined to ensure samples with variance in particle size. Secondly, an API processability study was performed using the model API, BSA. The API processability study included assessment of the blending step, the compaction step and the granulation step. This confirmed that the granulation process worked for both placebo and BSA formulations.

The second part of this project attempted to produce a sample set for calibration of a robust protein assay prediction model using NIR measurements of granulate. The granulate was produced using the granulation process that was developed in the first part of this project. Variation in particle size and BSA concentration was ensured this way. With the use of desiccators, the last granulate attribute regarding water content in the granulate was made controllable. The sample set was prepared and a dataset was acquired successfully. The dataset was presented and the variance found in it was demonstrated to be related to particle size, BSA concentration and water content. As a proof-of-concept, regression models for prediction of BSA concentration were calibrated and the different controlled variances in the dataset was utilized to simulate scenarios that would test the model calibrations' robustness.

Some unwanted sources of variances were identified in the down-scaled granulation process and in the sample preparation that calls for further investigation and if possible, mitigation:

1. SF variance was found within single riblets.
2. Other sources of variation in granulate morphology such as surface differences. A concern was described earlier regarding the possibility of granulate that consisted of small discs.
3. Other sources of variation in granulate morphology because of water content.
4. The aliquotation was found to be a potential source of systematic error as it was not completely successful in giving equal representativeness.
5. There were differences in the RH between some of the desiccators that should otherwise have been identical.

Perspectives

NIR technology has shown to be a valuable tool in development of this down-scaled dry granulation process. Some of the technologies that generally are used when developing a process and when determining product specifications are cumbersome. This project would like to propose NIR technology as a valuable tool to gain knowledge about a process. For example, this project used NIR to gain information about the granulate particle characteristics. The granulation research team at Novo Nordisk has a range of technologies to assess their process.

References

- Bhavishya Mittal, Chapter 4 - Pharmaceutical Unit Operations, Editor(s): Bhavishya Mittal, How to Develop Robust Solid Oral Dosage Forms from Conception to Post-Approval, Academic Press, 2017, Pages 69-95, https://doi.org/10.1016/B978-0-12-804731-6.00004-2

- Gerlach RW, Dobb DE, Raab GA, Nocerino JM, "Gy sampling theory in environmental studies. 1. Assessing soil splitting protocols", Journal of chemometrics, 2002-07, Vol.16 (7), p.321-328, DOI: 10.1002/cem.705

- Gregory E. Amidon, Pamela J. Secreast, Deanna Mudie, Chapter 8 - Particle, Powder, and Compact Characterization, Editor(s): Yihong Qiu, Yisheng Chen, Geoff G.Z. Zhang, Lirong Liu, William R. Porter, Developing Solid Oral Dosage Forms, Academic Press, 2009, Pages 163-186, ISBN 9780444532428, https://doi.org/10.1016/B978-0-444-53242-8.00008-4

- Higgins JP, Arrivo SM, Thurau G, Green RL, Bowen W, Lange A, Templeton AC, Thomas DL, Reed RA. 2003. Spectroscopic approach for on-line monitoring of particle size during the processing of pharmaceutical nanoparticles. Anal Chem 75: 1777–1785.

- Hu Changqin, Ni Zhen, Feng Yan-Chun. "Analyzing the Methods to Remove Artifacts Encountered in the Development of a NIR Quantitative Model for Powder Medicines", Journal of Analytical & Bioanalytical Techniques, 2010, DOI: 10.4172/2155-9872.1000114.

- Jean-Michel Roger, Jean-Claude Boulet, Magida Zeaiter, Douglas N. Rutledge, 3.01 - Pre-processing Methods, Editor(s): Steven Brown, Romà Tauler, Beata Walczak, Comprehensive Chemometrics (Second Edition), Elsevier, 2020, Pages 1-75, https://doi.org/10.1016/B978-0-12-409547-2.14878-4

- Olesen M, "Investigating a powder blending process - MSc pre-project on robust NIR calibration", UCPH Department of Food Science, 2022.

- Process Analytical Technology, (PAT) Initiative, U.S. Food and Drug Administration. Center for Drug Evaluation and Research Home Page (http://www.fda.gov/cder/OPS/PAT.html).

- Reich G. 2005. Near-infrared spectroscopy and imaging: Basic principals and pharmaceutical applications. Adv Drug Deliv Rev 57:1109–1143.

- Svante Wold, Kim Esbensen, Paul Geladi, Principal component analysis, Chemometrics and Intelligent Laboratory Systems, Volume 2, Issues 1–3, 1987, Pages 37-52, https://doi.org/10.1016/0169-7439(87)80084-9

- Zinchuk, Andrey V, Matthew P Mullarney, and Bruno C Hancock. “Simulation of Roller Compaction Using a Laboratory Scale Compaction Simulator.” International journal of pharmaceutics 269.2 (2004): 403–415. Web.

- F. Shikata, S. Kimura, Y. Hattori and M. Otsuka, “Real-time monitoring of granule properties during high shear wet granulation by near-infrared spectroscopy with a chemometrics approach”, RSC Advances Issue 61, 2017, https://doi.org/10.1039/C7RA05252A